

Regulatory T cell-derived enkephalin gates nociception

Élora Midavaine¹, Beatriz C. Moraes¹, Jorge Benitez¹, Sian R. Rodriguez¹, Joao M. Braz¹, Nathan P. Kochhar¹, Walter L. Eckalbar¹, Ana I. Domingos², John E. Pintar³, Allan I. Basbaum^{1*}, Sakeen W. Kashem^{4,5*}

Affiliations:

¹Department of Anatomy, University of California San Francisco, San Francisco, California, USA.

²Department of Physiology, Anatomy and Genetics, University of Oxford, Oxford, UK.

³Department of Neuroscience and Cell Biology, Rutgers Robert Wood Johnson Medical School, Piscataway, NJ, USA.

⁴Department of Dermatology, University of California San Francisco, San Francisco, CA, USA.

⁵Dermatology, Veterans Affairs Medical Center, San Francisco, California, USA.

*These authors contributed equally

Correspondence:

Allan I. Basbaum,
Chair and Professor, Department of Anatomy
University of California San Francisco
1550 Rock Hall, Room 345A, San Francisco, California, USA 94158
Email: allan.basbaum@ucsf.edu

Lead correspondence:

Sakeen W. Kashem
Assistant Professor, Dermatology
University of California San Francisco
1701 Divisadero, 3rd Floor, San Francisco, CA 94115
Email: sakeen.kashem@ucsf.edu

Keywords:

Pain, regulatory T cells, neuroimmunology, sex dimorphism, opioid, sensory neurons, enkephalin, meninges

Summary

T cells have emerged as sex-dependent orchestrators of pain chronification but the sexually dimorphic mechanisms by which T cells control pain sensitivity is not resolved. Here, we demonstrate an influence of regulatory T cells (Tregs) on pain processing that is distinct from their canonical functions of immune regulation and tissue repair. Specifically, meningeal Tregs (mTregs) express the endogenous opioid, enkephalin, and mTreg-derived enkephalin exerts an antinociceptive action through a presynaptic opioid receptor signaling mechanism that is dispensable for immunosuppression. We demonstrate that mTregs are both necessary and sufficient to suppress mechanical pain sensitivity in female, but not male, mice, with this modulation reliant on sex hormones. These results uncover a fundamental sex-specific, and immunologically-derived endogenous opioid circuit for nociceptive regulation with critical implications for pain biology.

Highlights

1. Gating of allodynia by meningeal Tregs is sex hormone-dependent
3. Treg-derived enkephalin modulates mechanical pain sensitivity, not inflammation
4. Delta opioid receptor on MrgprD⁺ sensory neuron mediates pain processing by mTregs

1 **Introduction**

2 Pain prevalence is significantly higher in women across multiple pain conditions
3 including nerve injury-induced neuropathic pain, musculoskeletal pain, fibromyalgia and
4 migraine¹. Gender disparities in pain are further evidenced by notable changes in
5 chronic pain severity during hormonal gender affirming care². Here, we identified a
6 previously unknown immunological mechanism that underlies sex differences in both
7 acute and chronic pain regulation.

8
9 Regulatory T cells (Tregs) are a subset of CD4⁺ T cells characterized by their
10 immunosuppressive function and the expression of the X-linked master regulatory
11 transcriptional factor *Foxp3*. In addition to their critical function in limiting inflammation,
12 Tregs are also major contributors to wound healing, they regulate stem cell turnover,
13 maintain metabolic homeostasis, facilitate placental implantation and promote maternal-
14 fetal tolerance⁸⁻¹⁶. In the context of nervous system injury, Tregs mitigate pro-
15 inflammatory cytokine interferon- α (IFN- α)-driven mechanical pain hypersensitivity,
16 suppress microglia-driven nociceptive processing and can reduce astrogliosis.
17 Additionally, they contribute to improving remyelination, thereby promoting tissue
18 repair¹⁷⁻²⁰. However, whether and how Tregs can directly alter neuronal activity is still
19 unknown.

20
21 Here, we demonstrate that meningeal regulatory T cells (mTregs) are essential
22 contributors to baseline mechanical sensitivity, and to the inhibition of mechanical pain
23 hypersensitivity (allodynia) after nerve injury, but only in female mice. Using a well-
24 established spared-nerve injury (SNI) model of neuropathic pain, we further show that
25 expanding mTregs can reduce nociceptive processing independently of Treg tissue
26 repair programs. We find that mTregs produce the endogenous opioid met-enkephalin,
27 with female mice exhibiting increased numbers of enkephalinergic mTregs. mTreg-
28 derived enkephalin is required for the suppression of mechanical pain hypersensitivity,
29 but not inflammation. This distinction reveals a novel Treg function that differs from their
30 well-established roles in immunological restraint and tissue repair.

31
32 The involvement of distinct opioid receptors in the peripheral (PNS) and central nervous
33 systems (CNS) in the regulation of different pain modalities is well documented. Delta
34 (δ OR) and mu (μ OR) opioid receptors are differentially expressed among neuronal
35 subsets and regulate mechanical or thermal pain processing, respectively²¹⁻²³.
36 Enkephalin can bind to both δ OR and μ OR, but preferentially engages the δ OR. Here
37 we demonstrate that the anti-allodynic effects derived from mTregs are mediated by the
38 δ OR that is expressed on the *Mas*-related G protein-coupled receptor member D
39 (MrgprD) subset of unmyelinated primary sensory neurons.

40
41 Given the pronounced sex differences observed in Treg-mediated suppression of
42 nociceptive processing, we further explored the determinants of this sex selectivity. Our
43 findings indicate that gonadal hormones, rather than sex chromosomes, play a key role
44 in modulating Treg suppression of nociceptive thresholds. Thus, we propose a novel
45 mechanism by which Tregs mediate the suppression of nociception, regulated by sex-
46 specific hormonal influences.

47 **Results**

48 **Sex-specific suppression of nociceptive thresholds by meningeal Tregs**

49 As the immune system has emerged as a central determinant driving sex differences in
50 pain sensitivity, we sought to investigate its contribution to nociceptive processing²⁴.
51 Tregs are a fundamental cell type essential for maintaining and restoring tissue
52 homeostasis. Here we initially focused on identifying Treg localization and function
53 within nervous system tissues. Using confocal microscopy and flow cytometry on whole
54 meningeal sheets, dorsal root ganglia (DRG), sciatic nerves, spinal cords (SC) and
55 brain, we localized Tregs to the meninges of the CNS, and to the leptomeninges of the
56 DRG (**Figure 1A-C**). To enhance the sensitivity of Treg detection within these organs,
57 we utilized the bright reporter signals from the double reporter *Foxp3*^{eGFP-Cre}
58 *ERT2*,*Rosa26*^{LSL-tdTomato} mice. Notably, and consistent with previous reports we observed
59 a more pronounced localization of Tregs in the lumbar and caudal segments of the
60 spinal cord meninges (**Figure 1A**)²⁵. In the DRG, as for most leukocytes other than
61 resident macrophages, Tregs predominated in the leptomeninges, proximal to the
62 dorsal roots entry zone, with sparse presence within the DRG parenchyma (**Figure**
63 **1B**)²⁶. By intravenous administration of a fluorescently-labeled CD45 antibody and using
64 flow cytometry, we distinguished intravascular Tregs from tissue Tregs (**Figure S1A**)²⁷.
65 We quantified the numbers of non-vascular, tissue Tregs in various organs within the
66 nervous and lymphoid systems. We will further refer to the SC meningeal and DRG
67 leptomeningeal Tregs as mTregs (**Figure 1C**). We observed minimal localization of
68 Tregs in peripheral nerves and did not detect any Tregs within the parenchyma of the
69 CNS in young, uninjured mice. We observed nearly equivalent numbers of tissue Tregs
70 between male and female mice across tissue (**Figure 1D**)¹⁸.

71

72 To assess the feasibility of site-specific depletion of mTregs, we performed intrathecal
73 (IT) injections of pegylated diphtheria toxin (pegDT) in *Foxp3*-DTR mice²⁸. Although an
74 IT injection of Evan's blue rapidly spreads through the SC meninges and DRG, into the
75 brain and to the draining cervical and lumbar lymph nodes, pegylated fluorescently
76 labeled molecules (pegDyLight 650) remain restricted to the SC meninges and to the
77 DRG (**Figure S2A-B**). Consistently, a single 20 ng dose of pegDT IT selectively
78 depleted >90% of SC and DRG mTregs in both male and female mice, but spared
79 Tregs located in the brain meninges, draining lymph nodes, spleen, and peripheral
80 nerves (**Figure 1E-F**). Importantly, *Foxp3*-DTR mice subjected to repeated IT
81 administrations of pegDT do not exhibit the significant weight loss, splenomegaly and
82 mortality that typically develops following systemic autoimmunity in *Foxp3*-DTR mice
83 induced by repeated intraperitoneal (IP) injections of diphtheria toxin (DT) (**Figure S2C-F**).
84 Clearly, the pegDT IT system offers a novel method for selective depletion of
85 mTregs while avoiding systemic inflammation.

86

87 We next evaluated behavioral outcomes in mice following mTreg depletion. A single
88 dose of pegDT IT induced a profound and prolonged decrease in mechanical thresholds
89 in naïve female but not male *Foxp3*-DTR mice (**Figure 1G-H**). Importantly, mechanical
90 thresholds in wildtype (WT) C57BL/6 mice treated with pegDT IT or *Foxp3*-DTR mice
91 treated with vehicle IT did not differ, ruling out pegDT or IT injections as the cause of the
92 sex-specific allodynia (**Figure S3A**). In addition to evaluating mechanical

93 hypersensitivity, which is conveyed by mechanosensitive unmyelinated and myelinated
94 primary afferent nerve fibers, we also assessed mice for noxious heat sensitivity
95 mediated by Trpv1^+ nociceptors, cold sensitivity that is mediated by Trpm8^+ nociceptors,
96 pin prick sensitivity mediated by $\text{A}\delta$ afferents and brush responses mediated by $\text{A}\beta$
97 fibers. Although depletion of mTregs selectively induced mechanical allodynia in
98 females, it did not impact any other sensory modality. Motor function tests using the
99 rotarod also did not differ in either sex (**Figure 1I and Figure S3A-H**). We conclude that
100 mTregs selectively suppress mechanical thresholds in a sex-dependent manner,
101 effectively preventing mechanical allodynia in a previously uninjured state.
102

103 ***Expansion of mTregs alleviates injury-induced mechanical allodynia
104 independently of tissue repair***

105 In addition to exploring mTreg role in mechanical sensitivity in uninjured mice, we
106 investigated whether mTreg can suppress allodynia following nerve injury. Using a well-
107 established spared nerve injury (SNI) model of neuropathic pain, we transected and
108 ligated the common peroneal and tibial nerve branches of the sciatic nerve, sparing the
109 sural nerve. This model induces chronic, unremitting, and permanent mechanical
110 hypersensitivity with a non-healing neuroma formation four weeks after the injury
111 (**Figure 2A-B**)^{29,30}. As mice with SNI exhibit mechanical thresholds at the limit of
112 detection with commercially available von Frey filaments, we conducted single fiber
113 testing using the lowest available 0.008 g von Frey filament. Again, mTreg depletion
114 increased allodynia following SNI in females, but not in males (**Figure 2C-D**).
115

116 We next asked whether expanding mTregs could alleviate the mechanical allodynia
117 independently of tissue repair. Tregs express the high affinity interleukin-2 receptor, IL-
118 2Ra, and low-doses of IL-2 can effectively expand Tregs in mice, a therapeutic
119 approach that has been used to treat autoimmune diseases in humans³¹. IT injections of
120 low-dose IL-2 successfully expanded mTregs in both male and female mice (**Figure
121 2F**). However, although mTreg expansion promoted significant anti-allodynia in SNI
122 female mice, it did not exhibit a similar effect in males (**Figure 2G-H**). It is noteworthy
123 that acute IT injection of IL-2, in uninjured mice, did not increase nociceptive thresholds,
124 suggesting that an IL-2 or Treg-based therapy could selectively improve neuropathic
125 pain without affecting basal nociceptive processing (**Figure S4A-B**). IL-2 injections and
126 mTreg expansion in mice with SNI likewise did not alter noxious cold or heat sensitivity,
127 again highlighting the specificity of the sensory modality modulation by mTreg in the
128 context of neuropathic pain (**S4C-E**).
129

130 ***Gonadal hormones, not sex chromosomes determine sex-selective, anti-
131 nociceptive function of mTregs***

132 Foxp3 is an X-linked gene, some of which escape X-inactivation. Moreover, random X-
133 inactivation has been suggested to be potentially altered during inflammatory state in
134 females³²⁻³⁴. To test whether sex chromosomes dosage contributes to our observed
135 phenotype, we used the Four Core Genotypes (FCG) mouse model in which gonadal
136 sex in mice is independent of sex chromosomes^{35,36}. FCG mice harbor a deficiency in
137 the sex determining region Y protein (Sry) on the Y chromosome and instead feature an
138 autosomal transgenic insertion of Sry . This genetic configuration enables the

139 discrimination of sex chromosome dose influence from the contribution of gonadal
140 hormones (**Figure 2I**). Both XX and XY chromosome gonadal female mice displayed
141 mTreg-mediated alleviation of mechanical allodynia after SNI; XX- and XY- gonadal
142 male mice did not (**Figure 2J-L**). Similarly, after mTreg depletion in *Foxp3*-DTR mice
143 crossed to the FCG system, we found that female specific gonadal hormones, but not
144 sex chromosome, mediate the mTreg suppression of nociceptive thresholds in the
145 absence of injury (**Figure 2M-N**). Based on our findings in both uninjured and chronic
146 injury states, we conclude that there is a profound and consistent sex hormone-
147 dependent contribution of mTregs to the modulation mechanical pain sensitivity.
148

149 **Regulatory T cells express the endogenous opioid peptide enkephalin**

150 To investigate the molecular mechanisms through which Tregs suppress nociceptive
151 thresholds, we first interrogated public genomic resources. We hypothesized that
152 meningeal tissue Tregs could exhibit an activated lymphoid Treg phenotype rather than
153 a resting Treg phenotype. Tregs have increased expression of the *Penk* gene, which
154 encodes for *Proenkephalin*, a peptide precursor of both Met- and Leu-enkephalin, in
155 various tissues including the nervous system, in both mice and humans^{19,37-39}. Here we
156 re-analyzed raw public RNA-seq data of activated Tregs, resting Tregs, as well as
157 activated and resting CD4⁺ *Foxp3*⁻ conventional T cells (Tconv)⁴⁰. Strikingly, in activated
158 versus resting Tregs, we observed a significant upregulation of *Penk* expression
159 (**Figure 3A**). We also investigated other opioid ligand and receptor genes but only
160 recorded a very sparse expression of other opioid-related genes among the CD4⁺ T cell
161 subsets (**Figure 3B**). Based on our prior experience defining mechanical sensitivity
162 through enkephalin- δ OR signaling²¹, we therefore focused on Treg expression of *Penk*.
163 By ATAC-seq analysis, we observed open chromatin regions of the *Penk* locus in
164 activated Tregs, but not in other CD4⁺ T cell subsets. This open chromatin was similar
165 to the open chromatin, promoter and enhancer regions of the developing forebrain, an
166 established enkephalin-producing area of the murine CNS (**Figure 3C**)⁴¹. By analyzing
167 the raw dataset from the Immunological Genome Project⁴², we also explored *Penk*
168 expression within cell populations of the immune system. We observed a strikingly
169 greater *Penk* expression in Tregs, compared to other immune cells (**Figure 3D**).
170 Furthermore, *Penk* expression in Tregs increase significantly following stimulation with
171 IL-2, compared to other common gamma chain cytokines (**Figure 3E**).
172

173 To establish whether Tregs indeed produce the endogenous opioid peptide enkephalin,
174 we screened commercially available anti-Met-enkephalin antibodies. Met-enkephalin
175 was chosen over leu-enkephalin as the latter can be cleaved from both proenkephalin
176 and prodynorphin peptides⁴³. These antibodies were validated using *Penk*^{-/-} mice as
177 negative controls. Figure 3F shows that mTregs produce met-enkephalin, but meningeal
178 CD4⁺ T cells and lymphoid Tregs produce very low levels even after cytokine
179 stimulation (**Figure 3F**). We validated this finding by generating *Penk*^{Cre};Rosa26^{tdTomato}
180 mice, which fate-labeled enkephalinergic cells. Consistent with our antibody finding, we
181 observed very similar number of enkephalinergic lineage (tdTomato positive) mTregs in
182 naïve mice. Very few lymphoid or intravascular Tregs were tdTomato labeled (**Figure**
183 **3G**). Most interestingly, female mice exhibited significantly greater numbers of
184 enkephalin-positive Tregs in the meninges, but not in the lymphoid organs. This

185 distinction suggests that Treg fate and function variation across the sexes may be organ
186 system specific (**Figure 3H**).

187
188 ***mTreg-derived enkephalin is required for suppressing nociceptive processing***
189 Using *Penk*^{Cre};Rosa26^{tdTomato} mice, we next investigated enkephalin lineage positive
190 cells in the meninges and the DRG. Interestingly, we observed a significant increase in
191 the representation of mTregs in the tdTomato-positive enkephalin subpopulation
192 compared to tdTomato-negative cells (**Figure 4A-B**). In order to manipulate the
193 enkephalin-producing immune cells, we generated bone marrow chimeric mice by
194 transplanting *Penk*^{Cre};Rosa26^{DTR} bone marrow into irradiated CD45.2 congenically
195 marked WT mice (**Figure 4C**). This strategy enables a selective DT-induced depletion
196 of hematopoietic enkephalinergic cells, that spares depletion of non-hematopoietic
197 enkephalinergic cells of the nervous system and the stroma. Importantly, CD4⁺ T cells
198 of the meninges are predominantly bone marrow-derived and exhibit a tissue circulatory
199 characteristic rather than acquiring tissue residency⁴⁴. Consistently, we found that
200 mTregs are indeed bone marrow-derived, similar to lymphoid Tregs, and differ from
201 spinal microglia and skin Langerhans cells, which are host-derived (**Figure S5A-C**).
202 pegDT IT administrations in *Penk*^{DTR}^{Δheme} chimeric mice decreased the number of
203 mTregs and led to profound mechanical hypersensitivity in female, but not male mice, in
204 both uninjured and nerve injured states (**Figure 4D-G**). We conclude that blood-derived
205 meningeal enkephalinergic cells gate mechanical hypersensitivity in females.

206
207 Having established a female-specific contribution of the bone marrow-derived
208 enkephalin system, we next used female mice to dissect the mechanism of pain
209 regulation by mTregs. To establish whether bone marrow-derived enkephalin is required
210 for the regulation of nociceptive thresholds, we generated bone marrow chimeras in
211 which *Penk* deficient bone marrow is transplanted into irradiated hosts, thus generating
212 *Penk*^{Δheme} mice. As predicted, these *Penk*^{Δheme} mice display decreased nociceptive
213 thresholds during uninjured state, compared to vehicle-injected *Penk*^{Δheme} mice, which
214 supports our conclusion that hematopoietic cell-derived enkephalin controls basal
215 mechanical sensitivity but only in females (**Figure 4H**).

216
217 We recognize that recombination-based selective ablation of enkephalin on Tregs,
218 using *Foxp3*^{Cre} or *Foxp3*^{Cre-ERT2} has multiple limitations and caveats. These include
219 systemic targeting of Tregs, including enkephalinergic Tregs in the skin, potential
220 compensatory *Penk* regulation upon constitutive ablation, potential side effects of
221 tamoxifen, potential stochastic deletion of *Penk* outside of Tregs in homozygote
222 Cre/Cre-ERT2 mice, and the impact of random X-inactivation on heterozygous mice³⁷.
223 In light of these concerns, we also generated mixed bone marrow chimeras using 1:1
224 ratio of *Foxp3*-DTR and *Penk*^{Δheme} bone marrow and implanted these chimeras in irradiated
225 WT mice. Intrathecal injection of pegDT into these mice results in ablation of *FoxP3*-
226 DTR Tregs; the remaining Tregs are left deficient for *Penk* (*Penk*^{ΔmTreg} mice) while
227 preserving other immune cell types. Importantly, this approach circumnavigated
228 potential depletion of any previously unrecognized non-hematopoietic cells that express
229 *Foxp3*. At baseline, uninjected mixed chimeric mice had similar mechanical thresholds
230 as *WT*^{Δheme} control chimeras. As predicted, pegDT IT injection led to mechanical

231 hypersensitivity in uninjured *Penk*^{ΔmTreg} but not *WT*^{Δheme} control mice and exacerbated
232 nerve injury-induced hypersensitivity (**Figure 4I-J**). Having shown that IL-2-induced
233 mTreg expansion and expression of enkephalin alleviates neuropathic pain, we next
234 investigated whether this could be mediated by the δOR, the preferred receptor for
235 enkephalin. In these studies, we co-administered IL-2 and naltrindole, a selective
236 antagonist of the δOR, and observed that IL-2-induced anti-allodynia was abolished
237 (**Figure 4K-L**). We conclude that mTreg-derived enkephalin is required for suppressing
238 mechanical pain hypersensitivity and that this suppression is mediated by the δOR.
239

240 ***Treg-derived enkephalin is dispensable for immune suppression***

241 Previously, Tregs have been shown to suppress hyperalgesia following nerve injury by
242 suppressing IFN- γ -induced primary afferent sensitization¹⁷. Thus, we hypothesized that
243 a potential mechanism by which Treg-derived enkephalin mediates the suppression of
244 nociceptive thresholds involves modulation of immunological responses. To address
245 this possibility, we tested the nociceptive thresholds of immunodeficient *Rag2*^{-/-} mice
246 which are missing both T and B cells and compared them to immunocompetent
247 littermates. In these studies, we mated *Rag2*^{+/+} mice and were surprised to observe
248 decreased nociceptive thresholds in the *Rag2*^{-/-} offspring compared to their *Rag2*^{+/+} and
249 *Rag2*^{+/+} littermates. This finding suggests that there may be a mechanism of Treg-
250 mediated control of nociceptive thresholds, which is independent of exaggerated
251 lymphocyte-driven inflammation (**Figure 5A**). Furthermore, consistent with this
252 conclusion, depleting macrophages through liposomal clodronate administration did not
253 reverse the mechanical allodynia observed in female mice deficient in mTreg (**Figure**
254 **5B**)⁴⁵.

255
256 We also used the *PenkDTR*^{Δheme} bone marrow chimeric mice to deplete all bone
257 marrow-derived enkephalin lineage cells and assessed their contribution to the
258 regulation of immune responses. Unlike *Foxp3*-DTR mice, we observed no changes in
259 mouse weight or spleen size in *PenkDTR*^{Δheme} bone marrow chimeric mice chronically
260 injected with systemic DT (**Figure S5D-E**). Furthermore, we also did not observe any
261 specific alterations in CD4⁺ T cell cytokine production after nerve injury in the meninges
262 or lymphoid organs. We conclude, therefore that peripheral enkephalin does not
263 contribute to T cell-driven inflammatory responses (**Figure S5F-G**).
264

265 We next investigated the contribution of Treg-derived enkephalin in the regulation of
266 conventional T cell proliferation. We assessed T cell suppression capacity by co-
267 culturing naïve conventional CD4⁺ T cells with either WT *Penk*^{+/+} or *Penk*^{-/-} Tregs. We
268 observed no difference in the suppressive capacity of *Penk*^{-/-} Treg compared to control
269 Tregs (**Figure 5C-D**). Next, we transplanted equal amounts of CD45.1 *Penk*^{+/+} or
270 CD45.2 *Penk*^{-/-} CD4⁺ T cells into *Rag2*^{-/-} mice and performed SNI to measure chimerism
271 of congenic markers among CD4⁺ T cells. We did not observe a competitive advantage
272 or disadvantage amongst *Penk*^{-/-} CD4⁺ T cells across various tissues (**Figure 5E-G**).
273 Restimulating harvested T cells from distinct tissues with PMA/Ionomycin revealed no
274 differences in T cell differentiation across Tregs, T helper 1 (Th1) and Th17 subsets
275 between the *Penk*-sufficient or deficient T cells (**Figure 5H** and **Figure S5H-I**). In
276 addition, we noticed no difference in weight, health, or spleen size between *Penk*^{Δheme}

277 and *WT*^{Δheme} bone marrow chimeric mice further revealing that peripheral enkephalin
278 has a very limited, if any, role in the suppressing of systemic inflammatory responses
279 (**Figure S5J-K**).
280

281 Finally, using an adoptive transfer-based graft versus host disease (GVHD) model, we
282 assessed whether Treg-derived enkephalin is required for suppressing immune
283 responses. As expected, we observed a profound Th1 response in mice transferred with
284 activated Tconv alone. However, mice that received additional transfers of either
285 *Penk*^{+/+} or *Penk*^{-/-} Tregs equally suppressed Th1 responses, reduced GVHD severity
286 and mitigated weight dysregulation (**Figure 5 I-J and S5L-N**). In summary, we conclude
287 that Treg-derived enkephalin does not contribute to any inflammatory response restraint
288 mechanism. Rather, we conclude that Tregs can suppress pain sensitivity through a
289 mechanism that is independent of their function in immunosuppression.
290

291 ***Delta opioid receptor signaling on MrgprD⁺ primary afferent DRG neurons is***
292 ***required for the anti-allodynic function of mTregs***

293 Enkephalin is a potent agonist at the δOR, and, to a lesser extent the μOR. In our
294 previous studies, we demonstrated the divergence of expression and function of δOR
295 and μOR in mediating distinct pain modalities. Specifically, δOR is expressed on
296 nonpeptidergic IB4⁺ unmyelinated as well as myelinated primary afferents and
297 selectively regulates mechanical thresholds and nerve injury-induced mechanical
298 hypersensitivity²¹. Conversely, the μOR is expressed on Trpv1⁺ nociceptors and
299 selectively regulates thermal hyperalgesia. In addition, a spinal δOR can dampen
300 mechanical hypersensitivity by inhibiting the excitability of somatostatin-positive dorsal
301 horn interneurons²³.
302

303 To assess the requirement of PNS or CNS δOR circuits in coordinating the anti-
304 allodynic effect of mTregs, we intravenously injected *Oprd1*^{+/+} control or *Oprd1*^{fl/fl} mice
305 with AAV.PHP.S-CAG-Cre or AAV.PHP.eB-CAG-Cre. This approach selectively
306 introduces Cre recombinase and targets deletion of δOR into to the PNS (DRG) or CNS
307 (spinal cord and brain), respectively (**Figure 6A**). Three weeks after the AAV injection,
308 we performed SNI and four weeks later administered IL-2. Mice selectively lacking δOR
309 in the PNS lost the capacity to respond to the anti-allodynic effect of IL-2, but the effects
310 of IL-2 were preserved in mice lacking δOR in the CNS (**Figure 6B-C**). We conclude
311 that a sensory neuron-expressed, presynaptic δOR coordinates mTreg suppression of
312 mechanical pain hypersensitivity.
313

314 Next, we identified the specific sensory neuron subset that coordinates the anti-
315 nociception mediated by mTreg-derived enkephalin. Previous studies of δOR
316 expression on DRG sensory neurons using *Oprd1*^{eGFP} reporter mice revealed that
317 approximately half of the reporter-positive cells in the DRG are myelinated neurons,
318 while approximately 36% are IB4⁺ non-peptidergic neurons expressing the MrgprD
319 receptor. Using established single cell RNA sequencing resources, we found that the
320 MrgprD⁺ subset of DRG sensory neurons not only expresses *Oprd1*, but also other
321 receptors for Treg ligands, including *Il10ra* and *Icosl*, which have been implicated in
322 suppression of pain thresholds⁴⁶⁻⁴⁸ (**Figure 6D**). The total proportion of sensory neurons

323 expressing the *Oprd1* transcript matches previous data using *Oprd1^{eGFP}* reporter mice
324 (**Figure 6E**). Our subsequent flow cytometry-based profiling of *Oprd1^{eGFP}* reporter
325 expression on DRG cells confirmed GFP expression specifically on IB4⁺ CD45⁻ Thy1⁺
326 sensory neurons, which corresponds to the MrgprD⁺ nonpeptidergic nociceptive neuron
327 population. Importantly, the flow analysis confirmed the absence of GFP expression on
328 broadly defined CD45⁺ CD90.2⁺ IB4⁻ lymphoid cells and CD45⁺ CD11b⁺ CD90.2⁻ IB4⁻
329 myeloid cells (**Figure 6F**). We also confirmed the absence of GFP expression on
330 microglia as well as on immune cells profiled from the draining lymph nodes (data not
331 shown)²³. Based on this selective *Oprd1* expression profile, we generated mice in which
332 MrgprD⁺ neurons lack the δOR (*MrgprD*^{Cre-ERT2}, *Oprd1*^{f/f}). Female *MrgprD*<sup>Cre-
333 ERT2</sup>, *Oprd1*^{f/f} mice, but not their male counterparts, exhibited exaggerated mechanical
334 hypersensitivity after SNI compared to tamoxifen-injected sex-matched littermate
335 controls (**Figure 6G-H**). Female mice lacking δOR on MrgprD⁺ sensory neurons and
336 treated with IL-2 IT four weeks following SNI displayed a complete deficiency in IL-2
337 anti-allodynic efficacy (**Figure 6I-J**). We conclude that, the enkephalin receptor δOR,
338 expressed specifically by MrgprD⁺ sensory neurons, mediates the anti-nociceptive
339 function of mTregs.

340

341

342 **Discussion**

343 In this report, we describe a novel, sexually dimorphic mechanism for pain regulation by
344 the immune system. Using a range of site-selective targeting strategies to deplete or
345 expand Tregs within the recently recognized borders of the nervous system, specifically
346 the meninges, we find that meningeal Tregs (mTregs) can profoundly modulate
347 mechanical hypersensitivity. Strikingly, this pain regulatory function of mTregs is sex-
348 specific and controlled by gonadal hormones. Although proenkephalin expression by
349 Tregs has been observed in sequencing studies, its functional relevance to nociception
350 had not been explored. Here, we demonstrate that enkephalin secreted by mTregs acts
351 on δ-opioid receptors (δOR) on primary sensory neurons to selectively modulate
352 mechanical sensitivity. Our findings provide the first mechanism of Treg-mediated
353 suppression of nociception and establish regulatory T cells as key sentinels of pain
354 homeostasis.

355

356 To assess for sex differences in transcriptional identity after nerve injury, primary
357 afferent neurons, including those expressing MrgprD, have recently been sorted for
358 deep RNA sequencing⁵². Surprisingly, very few differences were found between the
359 sexes, suggesting a lack of a strong intersection of sex and injury in the transcriptional
360 identity of peripheral neurons. The lack of transcriptional differences may also suggest
361 that non-neuronal cells may be a primary determinant of sex-selective pain modulation.
362 Indeed, preclinical research has demonstrated the involvement of T cells in driving pain
363 phenotypes in female mice⁵³. Additionally, human leukocyte antigen (HLA) risk alleles
364 have been identified for human chronic pain conditions, further suggesting a potential
365 role for T cells in pain modulation^{24,54}.

366

367 Regulatory T cells display broad tissue supportive roles that extend beyond their
368 originally described function in suppressing inflammation^{8,11,12,20}. A major advantage of

369 our analysis is that we utilized a site-selective mTreg ablation strategy that preserved
370 peripheral Tregs and avoided systemic inflammation. Using this approach, we identify a
371 novel, sex-specific mechanism by which Tregs modulate nociceptor activity to regulate
372 pain sensitivity in the context of health and nerve injury. Although, proenkephalin-
373 expressing Tregs have been identified in various tissues, their functional assessment
374 has been limited^{19,37,38}. Somewhat paradoxically, a recent pre-print study demonstrated
375 a small but statistically significant decrease in basal heat sensitivity in both female and
376 male mice conditionally depleted for *Penk* expression in systemic Tregs. Mechanical
377 thresholds and other sensory modalities were however not examined⁵⁵. In distinct
378 contrast, we uncover a sensory modality selective function of mTreg that is consistent
379 with prior findings of δ OR agonism, namely providing relief of mechanical but not heat
380 pain^{21,56}. Whether mTregs tonically restrain nociception is difficult to conclude. Our
381 finding of increased basal sensitivity in *Rag2*^{-/-} or *Penk*^{Aheme} mice, is supportive of this
382 hypothesis, however, alternative possibilities exist. It is conceivable that mTreg
383 deficiency could lead to inflammation, which may alter nociceptor sensitivity.
384 Additionally, the endogenous opioid signaling pathway may have a role in opioid
385 induced analgesia. It is significant that naloxone, a non-selective opioid receptor
386 antagonist IV injection, does not induce pain in healthy individuals. Whether
387 experiments in uninjured female mice have been performed is unclear⁵⁷.
388

389 Our observations suggest that sex hormones, rather than sex chromosomes, are the
390 main drivers of mTreg-induced anti-nociception. While the specific sex hormones
391 involved in regulating mTreg function in pain remain unclear, previous studies have
392 implicated estrogen and progesterone in modulating neuropathic pain associated with
393 SNI⁴⁹. Estrogen administration increases *Penk* expression in the whole spinal cord⁵⁸.
394 Additionally, in CD4⁺ T cells, the estrogen receptor engages conserved non-coding
395 sequences (CNS) in *Foxp3* enhancer regions⁵⁹. Importantly, we reveal an anti-
396 nociceptive role for regulatory T cells that is distinct from their well-established functions
397 in immune suppression and tissue repair. Furthermore, we demonstrate that this
398 mechanism operates within nervous system tissues, at a site distant from the peripheral
399 nerve injury, highlighting the immune system's remarkable ability to modulate
400 nociception.
401
402
403
404
405
406
407
408
409
410
411
412
413
414

415

416

417

418 **Methods**

419

420 **Mice**

421 All mouse experiments were approved by UCSF Institutional Animal Care and Use
422 Committee and conducted in accordance with the guidelines established by the
423 Institutional Animal Care and Use Committee and Laboratory Animal Resource Center.
424 All mice experiments were performed on age-matched adult male and female mice at a
425 starting age between 8 and 14 weeks old. Littermate controls were used for all
426 experiments when feasible. Mice were bred in-house and backcrossed over 10
427 generations to C56BL/6 breeders obtained from Jackson labs. Experimental mice were
428 co-housed to maintain the same microbiome. They were maintained in a temperature
429 (21°C) - and light (12h light/dark cycle)-controlled environment and were provided with
430 food and water *ad libidum*. The following mouse strains are used: C57BL/6J (JAX
431 #000664), *Foxp3*-DTR (B6.129(Cg)-*Foxp3*tm3 (Hbegf/GFP)Ayr/J, JAX# 016958),
432 *Foxp3*^{eGFP-Cre-ERT2} (Foxp3tm9 (EGFP/cre/ERT2)Ayr/J; JAX#016961), Ai9 (B6.Cg-
433 *Gt(ROSA)26Sor*^{tm14(CAG-tdTomato)Hze}/J; JAX#007914), Four Core Genotypes (B6.Cg-
434 Tg(Sry)2Ei Srydl1Rlb T(XTmsb4x-Hccs;Y)1Dta/ArnoJ; JAX#010905), *Penk*-IRES2-
435 Cre(B6;129S-Penk^{tm2}(cre)Hze/J; JAX#025112), Rosa26-ISL-iDTR (CBy.B6-
436 *Gt(ROSA)26Sortm1(HBEGF)Awai*/J;JAX#008040),CD45.1 (B6.SJL-Ptpca Pepcb/BoyJ;
437 JAX# 002014), B6C3F1/J (JAX#100010), *Rag2*^{-/-} (B6.Cg-*Rag2*tm1.1Cgn/J;
438 JAX#008449), Mrgprd-CreERT2 (Mrgprd^{tm1.1(cre/ERT2)Wql}/J; JAX# 031286),
439 Oprd1fl/fl (B6;129-Oprd1tm1.1Cgrf/KffJ; JAX# 030075), DOR-eGFP (B6;129S2-
440 Oprd1tm2Kff/J; JAX#029012). *Penk*^{-/-} were kindly provided by Dr. John Pintar on a
441 C57BL/6 background (MGI 3628668)⁶⁰. *Foxp3*-DTR (X-linked) was mated with male
442 Four Core Genotypes XY^{Sry}-Sry^{Tg} and the X^{*Foxp3*-DTRYSry}-Sry^{Tg} male mice were mated to
443 homozygous *Foxp3*-DTR female mice.

444

445 **Bone marrow transplantation**

446 CD45 mismatched host recipient mice were irradiated at 550 cGy twice, 5 hours apart
447 and injected retro-orbitally with 5x10⁶ cells from the bone marrow of CD45.1 WT,
448 *Penk*^{Cre};Rosa26^{DTR} *Penk*^{-/-} or a 1:1 mix of *Foxp3*-DTR and *Penk*^{-/-} sex-matched 7-10
449 week old mice. Mice were kept on doxycycline chow for the first week (Bioserv #S3888)
450 and chimerism was assessed at 8 weeks post-transplant.

451

452 **Pharmacological interventions**

453 Animals were randomly assigned to vehicle control or treatment group. Pegylated
454 diphtheria toxin (pegDT) was a generous gift from Ana I. Domingos and generated as
455 previously described⁶¹. pegDT (20 ng) or corresponding phosphate-buffered saline
456 (PBS) control were injected intrathecally (IT) in a volume of 5 μ L in naive mice below
457 lumbar level L4. All intrathecal injections were performed in non-anesthetized, lightly
458 restrained mice and injections were validated by a sudden flick of the tail. Of note, the 5-
459 10 μ L injection distributes predominantly to the lumbo-sacral cord given lidocaine IT
460 injection at that segment paralyzes the hindpaws but not forepaws. Non-pegylated

461 diphtheria toxin (30 ng/g, Sigma Cat#322326) or corresponding saline control were
462 administered in a volume of 200 μ l every three days intraperitoneally (IP). IL-2 (0.1 μ g,
463 Peprotech, Cat# 212-12) or PBS vehicle control were administered daily for three
464 consecutive days IT. Selective δ OR agonist, [D-Ala2]-Deltorphin 2 (15 μ g, Abcam Cat
465 #ab120708, CAS 122752-16-3) and selective δ OR antagonist, naltrindole (5 μ g, Sigma
466 Cat# N115) administrations were performed 30 min before behavior experiments.
467

468 **Tamoxifen injections**

469 *Mrgprd*^{CreERT2}; *Oprd1*^{f1/f1} and *Foxp3*^{eGFP-Cre-ERT2}; *Rosa26*^{tdTomato} mice were injected IP with
470 tamoxifen (Sigma Cat #5648) 100 mg/kg in corn oil (Sigma Cat #8267) for five
471 consecutive days to induce Cre-mediated recombination.
472

473 **Intrathecal dye tracing**

474 Naive mice were intrathecally injected with 5 μ L of Evans Blue 1% solution (Sigma, Cat
475 #E2129) or pegylated DyLight 650-4xPEG NHS Ester (Thermo Fischer, Cat #62274).
476 24 hours post-injection, mice were anesthetized with avertin and euthanized by
477 decapitation. Spinal cord and brain meninges, spinal cord, brain, dorsal root ganglia and
478 trigeminal ganglia, sciatic nerve and lymph nodes were assessed for dye uptake.
479

480 **Animal behavior**

481 For all behavioral tests, the experimenter was blind to genotype and treatment and
482 performed during the light cycle. The project utilized both male and female
483 experimenters but a predominant number of experiments were performed by a female
484 investigator⁶².
485

486 **von Frey measurement of mechanical hypersensitivity**

487 Mice were acclimatized once to the von Frey apparatus for two hours. The lateral
488 plantar surface of the ipsilateral and contralateral hind paws (sural innervation) was
489 stimulated with von Frey hairs of logarithmically increasing stiffness (Stoelting Cat #
490 58011). Animals were habituated on a wire mesh for 1 hour, after which they were
491 tested with von Frey filaments (0.008, 0.02, 0.04, 0.07, 0.16, 0.4, 0.6, 1, 1.4, 2, 4 and 8
492 g) using the Dixon up-down method^{63,64}. The von Frey hairs were held for 3 sec with
493 intervals of several minutes between each stimulation. For the Dixon up-down method
494 we recorded 2 days of baseline mechanical sensitivity which were averaged. After SNI,
495 nearly all mice reached a 50% paw withdrawal threshold of the lowest filament (0.008
496 g), thus we utilized a single fiber method of testing to achieve resolution of allodynia
497 severity. Mice were stimulated 10 times with the 0.008 g filament. The filament was
498 applied for 3 seconds and the number of positive responses across the 10 stimulations
499 were registered as percent nociceptive responses.
500

501 **Hargreaves measurement of heat hypersensitivity**

502 Mice were acclimatized for 30 min in plexiglass cylinders. The mice were then placed on
503 the glass of a Hargreaves apparatus and the latency to withdraw the paw from the heat
504 source was recorded. Each paw was tested three times and latencies were averaged
505 over the trials.
506

507 **Acetone induced cold sensitivity**

508 Mice were habituated for 60 min on a mesh in plexiglass cylinders. A syringe was used
509 to spray 50 μ l of acetone (Thermo Scientific Cat # 423240010) onto the plantar surface
510 of the paw and the behaviors were video recorded for 30 seconds after each trial using
511 a Sony HDR-CX440 camera. The left hind paw was tested five times and positive
512 responses included withdrawals, shakes, licks and jumps. Results are displayed as the
513 total number of behaviors across the five trials.

514

515 **Tail flick measurement of heat hypersensitivity**

516 Mice were placed in a restrainer and 2 cm of the tip of the tail was submerged in a 52°C
517 water bath. The latency (seconds) to withdraw the tail from the water was recorded. A
518 cut-off of 15 s was set to prevent tissue damage and testing was performed with
519 intervals of several minutes between each stimulation. Mice were tested three times and
520 withdrawal latencies were averaged.

521

522 **Hot plate measurement of heat hypersensitivity**

523 Mice were acclimated to the testing environment as described above. The hot plate
524 temperature was set to 52°C. The mouse was placed on the plate and the latency to
525 shake, lick or bite a hindpaw was scored. A cut-off of 20 s was set to prevent tissue
526 damage.

527

528 **Pin prick withdrawal test**

529 Mice were habituated for 60 min on a mesh in plexiglass cylinders. A 27G needle was
530 gently applied onto the hindpaws, with minutes between each stimulation for a total of 5
531 stimulations per paw. Mice were scored as follow: 1: brief withdrawal, 2: mice lifting their
532 paw for 1 sec, 3: mice lifting their paw for 2 sec or shake, 4: lick. Results are displayed
533 as the total number of behaviors across the five trials.

534

535 **Brush withdrawal test**

536 Mice were habituated for 60 min on a mesh in plexiglass cylinders. A 5-0 brush was
537 gently applied onto the hindpaws, with minutes between each stimulation for a total of 5
538 stimulations per paw. Mice were scored as follow: 1: brief withdrawal, 2: mice lifting their
539 paw for 1 sec, 3: mice lifting their paw for 2 sec or shake, 4: lick. Results are displayed
540 as the total number of behaviors across the five trials.

541

542 **Rotarod**

543 Mice were acclimatized to the testing room and trained by placing them on an
544 accelerating rotarod for a maximum of 60 seconds at low speed, three times with
545 training taking place on two consecutive days. Latency to fall was measured with a
546 cutoff of 300 seconds. The procedure was repeated three times and latencies averaged
547 across trials.

548

549 **Spared Nerve injury**

550 We employed an established, robust and reliable spared nerve injury (SNI) model to
551 induce a chronic neuropathic injury⁶⁵. This model utilizes non-healing surgical
552 intervention on two branches of the sciatic nerve (the common peroneal and tibial

553 branches), while sparing the third branch (the sural branch) for sensory testing on the
554 lateral portion of the hindpaw. Briefly, mice were anesthetized with isoflurane (3% for
555 induction and 1.5% for maintenance, mixed with oxygen). The fur on the left hind leg
556 was shaved and disinfected with 3 passages of alcohol and iodine solution,
557 alternatively. A 1 cm incision was performed on the upper thigh skin, near the division
558 point of the sciatic nerve. A 2% lidocaine solution was applied and the biceps femoris
559 muscle was gently separated through a blunt opening to reveal the sciatic nerve's
560 common peroneal, tibial, and sural branches. The common peroneal and tibial nerves
561 were ligated with non-dissolvable 8-0 silk sutures (Fine Science Tools Cat # 12052-08).
562 Subsequently, a 2 mm segment from both the common peroneal and tibial nerves was
563 transected, ensuring the sural nerve remained undisturbed. The muscle and the skin
564 were stitched using 6-0 sutures (Henry Schein Surgical suture Cat #101-2636), and the
565 skin was further sealed with a tissue adhesive (3M Vetbond Cat # 1469SB), after an
566 ethanol solution application. Mice were kept on heating pad until they regained
567 consciousness and demonstrated stable, balanced locomotion. Mice were transferred
568 into their home cage and observed meticulously for the next two days.
569

570 Immunohistochemistry

571 Avertin-anesthetized mice were transcardially perfused with 10 ml of 1x PBS followed
572 by 30 ml of 4% paraformaldehyde (PFA, Thermo Scientific Cat # 119690010) diluted in
573 PBS. After perfusion, spinal cord, sciatic nerves, lymph nodes, spleens, brains and
574 DRG were collected, postfixed in 4% PFA solution at 4°C for 5□h and then
575 cryoprotected in 30% sucrose in PBS at 4°C.
576

577 Spinal meninges were harvested from fixed spinal cords. Spinal cords were transferred
578 in PBS and meninges were gently peeled into a single sheet onto a microscope slide
579 after a longitudinal hemisection of the spinal cord. Brain meninges were similarly
580 harvested from the skull. Frozen tissues were embedded at -35°C in O.C.T. compound
581 and 30□μm transverse spinal cord sections were generated using a Leica SM220R
582 sliding microtome and 20 μm DRG sections were generated using a cryostat (Thermo
583 Fisher Scientific) on SuperFrost Plus slides. Spinal cord sections were processed as
584 free-floating. Sections were blocked (10% NGS, 1% BSA, 0.05% Tween-20, 0.1% Triton
585 X-100 in PBS) and incubated in 0.3 M glycine containing 0.2% Tween 20. Sections
586 were labeled in blocking buffer for 24 hours at 4°C. Slides were coverslipped with
587 Fluoromount-G (Thermo Fisher Scientific). Fluorescence images were acquired using
588 an Olympus FV3000 confocal microscope and quantified using ImageJ (Fiji).
589

590 Tissue clearing

591 Whole DRG or spinal cords from *Foxp3*^{eGFP-Cre-ERT2};Ai9 mice were cleared after PFA
592 fixation using SHIELD tissue clearing (LifeCanvas PCK-500)⁶⁶. Tissues were washed in
593 PBS then processed as previously described⁶⁶. Briefly, the tissues were incubated in
594 epoxy solution (SHIELD OFF) for 10 hours at 4°C with gentle shaking then incubated
595 overnight at 37°C in SHIELD ON-Epoxy solution for epoxy crosslinking. DRG were then
596 further incubated in SHIELD ON solution for 10h and delipidated for two days (DRG) to
597 five days (spinal cord) at 45°C with shaking then washed with PBS. Whole mount DRG

598 and spinal cords were acquired in FocusClear reflexive index matching solution
599 (CelExplorer, FC-102).

600

601 **Tissue digestion**

602 Mice were injected intravenously with 50 μ l of anti-ARTC2 nanobody (Biolegend Cat #
603 149802) in 200 μ L of PBS 30 minutes before euthanasia to protect Treg during harvest
604 from purinergic-mediated cell death⁶⁷. 5 minutes before harvest mice were injected
605 intravenously with 6 μ g of FITC-conjugated anti-CD45 antibody to label blood immune
606 cells in 200 μ L of PBS²⁷. Avertin-anesthetized mice were decapitated, and spinal cord
607 meninges, brain meninges, L4-6 DRG, sciatic nerves, lymph nodes, brains and spleens
608 were harvested. Spinal cord meninges, brain meninges, DRG, sciatic nerves and brains
609 were crushed with the back of a 3ml syringe in a serrated 24 well plate and triturated in
610 digestion media (Liberase TM (0.208 WU/ml) (Roche Cat # 054010200001) and DNase
611 I (40 ug/ml) (Sigma Cat # DN25) in 1.0 ml cRPMI (RPMI supplemented with 10%
612 (vol/vol) fetal bovine serum (FBS), 1% (vol/vol) HEPES, 1% (vol/vol) Sodium Pyruvate,
613 1% (vol/vol) penicillin-streptomycin). They were digested for 30 min at 37°C, 220 RPM
614 and triturated every 15 minutes. Digested samples were again triturated and passed
615 over a 40 μ m cell strainer and any remaining tissue pieces mashed through the cell
616 strainer. Cell strainers were flushed with staining media (PBS w/o Mg²⁺ and
617 Ca²⁺ supplemented with 3% FBS, 2 mM EDTA and 0.05% NaN₃). Single-cell
618 suspensions were centrifuged at 500 g at 4°C, washed and resuspended in staining
619 media. Spleens and lymph node immune cells were obtained by mashing the tissues
620 over a 40 μ m cell strainer and washed with staining media.

621

622 **Cell stimulation**

623 Isolated single cell suspensions were incubated for 4 hr at 37°C in complete IMDM
624 (supplemented with 10% FBS, 2 mM L-glutamine, 10 mM HEPES, 1% sodium pyruvate,
625 1% penicillin-streptomycin, 50 μ M 2-mercaptoethanol) with (phorbol 12-myristate 13-
626 acetate) PMA, Ionomycin in the presence of Brefeldin A and Monensin (Tonbo, TNB-
627 4975).

628

629 **Flow cytometry**

630 Single-cell suspensions were stained in a 96 well plate. Briefly, they were washed with
631 250 μ L of staining media and stained with viability dye (1:500) and cell surface
632 antibodies (1:100) in 100 μ L of staining media with Fc shield (1:100). Samples were
633 washed twice in staining media and stained for intracellular cytokines or for Foxp3
634 according to manufacturer recommendations with BD Cytofix/Cytoperm
635 Fixation/Permeabilization Kit (BD 554714, AB_2869008). Samples were further stained
636 with conjugated intracellular antibodies (1:100) overnight at 4°C in BD
637 permeabilization/wash buffer. Samples were washed with permeabilization/wash buffer
638 twice and resuspended in 200 μ L of staining media. For visualization of both tdTomato
639 reporter signal and intranuclear Foxp3 signal, cells were fixed in 200 μ L of freshly
640 prepared 2% formaldehyde (EM grade) in PBS for 60 minutes exactly and washed with
641 eBioscience Permeabilization buffer (eBioscience Foxp3 perm-kit) and stained
642 overnight in 1x eBioscience Permeabilization buffer at 4°C⁶⁸. Cells were washed twice
643 in the buffer and resuspended in staining media. For Met-enkephalin staining, we

644 screened multiple commercially available antibodies and selected an antibody that
645 showed positive staining in wildtype mTreg but not *Penk*^{-/-} mTreg. The antibody was
646 conjugated to fluorescent phycoerythrin with Lightning-link conjugation kit (ab102918)
647 and utilized after cell stimulation and intracellular cytokine staining. Cells were counted
648 with 50 μ L of counting beads (Thermo Fisher Scientific Cat # C36950) and samples
649 were analyzed using a BD FACSCanto2 or BD FACS Aria Fusion flow cytometer (BD
650 Biosciences). Positive and negative selection gates were set using fluorescence minus
651 unstained cells. For negative control of enkephalin staining, *Penk*^{-/-} samples were used
652 for gating. Fluorescence intensity distribution was analyzed using FlowJo 10 software
653 (BD Biosciences). Antibodies for flow cytometry are listed in the resource table. Lineage
654 exclusion markers include viability dye, CD11b (to exclude myeloid cells), B220 (to
655 exclude B cells), Ter119 (to exclude red blood cells).

656

657 **Cell sorting**

658 Spleens were mashed on a cell strainer and cells were pelleted at 500 g for 10 min at
659 4°C. Cells were stained for viability and lineage exclusion markers, in addition to CD45,
660 CD4, CD45RB to stain naïve Tconv and CD25 to stain Tregs. Cells were pelleted,
661 washed and incubated with CD4 negative selection beads and purified on a LS
662 magnetic column (Miltenyi Biotec). Cells were double sorted in BD FACS Aria Fusion for
663 Singlet, Live, CD45⁺ CD4⁺ CD45RB⁺ CD25⁻ for Tconv or Singlet, Live, CD45⁺ CD4⁺
664 CD25⁺ CD45RB⁻ for Treg into complete IMDM.

665

666 **T cell suppression assay**

667 Sorted Tconv from lymphoid organs of CD45.1 female mice were labeled with cell trace
668 violet (Thermo-Fisher, Scientific #C34571) according to manufacturer instructions.
669 0.25x10⁵ Tconv per well were cultured with distinct dilution of Treg from CD45.2 WT or
670 *Penk* deficient lymphoid organs. Cells were then washed and resuspended with mouse
671 anti-CD3/CD28 Dynabeads at a 1:1 ratio of beads to Tconv. Cells were incubated for 96
672 hours in a humidified incubator at 37°C. Cells were washed and resuspended in staining
673 media and suppression ratio was calculated by dividing the percent proliferated cells
674 from incubated Tconv⁺ Treg samples by percent proliferated cells from Tconv only
675 samples⁶⁹.

676

677 **T cell adoptive transfer**

678 *Competition assay*

679 1x10⁶ negatively selected bulk CD4⁺ T cells from WT female and *Penk* deficient
680 lymphoid organs were transplanted into female *Rag2*^{-/-} mice. SNI was performed and
681 organs were collected 28 days later for cell stimulation and flow cytometry.

682

683 *Graft versus host disease (GVHD)*

684 GVHD was established as previously described. Briefly, WT or *Penk* deficient female
685 mice bone marrow was transplanted into MHC mismatched B6C3F1/J female mice to
686 activate T cells. 0.25x10⁶ sorted WT Tconv were transplanted into male *Rag2*^{-/-} mice to
687 induce chronic GVHD either without Tregs or in the presence of 0.125 x10⁶ WT or *Penk*
688 deficient Tregs. Mice were measured for weight changes and GVHD score. Mice were
689 euthanized then harvested for cytokine secretion assay by flow cytometry^{70,71}. GVHD

690 scoring is as follows: 0 = no signs of GVHD, 1 = visible signs of GVHD (hunching,
691 lethargy, ruffled fur), 2 = no weight gain, 3 = 0-5% weight loss, 4 = >5% weight loss.
692 One Tconv mouse did not survive for harvesting for cytokine stimulation.
693

694 **Analysis of sequencing data**

695 *Bulk RNA-seq*

696 Raw files GSM4677053-064 from GEO dataset GSE154680, and all files from GSE
697 GSE180020 were gathered and aligned using STAR for uniquely mapped reads
698 (outFilterMultimapNmax 1–outFilterMatchNmin 30–alignIntronMin 20–alignIntronMax 1–
699 0000). Data was annotated with GENCODE GRCm38/mm10 genome assembly. Raw
700 count tables were normalized by median of ratios method with DESeq2 package from
701 Bioconductor to analyze for differential expression.
702

703 *ATAC-seq*

704 Fastq files were gathered from SRR12264679-94 from GSE154680. Raw reads were
705 mapped to the mouse mm10 genome assembly using STAR alignment (--
706 outFilterMismatchNoverLmax 0.04 --outFilterMismatchNmax 999 --
707 alignSJDBoverhangMin 1 --outFilterMultimapNmax 1 --alignIntronMin 20 --
708 alignIntronMax 1000000 --alignMatesGapMax 1000000). Bam files were generated by
709 STAR. PCR duplicates were removed by Picard, and peak calling performed using
710 MACS2 (--keep-dup 1 --bw 500 -n output --nomodel --extsize 400 --slocal 5000 --llocal
711 100000 -q 0.01) PMID: 22936215). To generate bigwig files for ATAC-seq datasets, all
712 aligned bam files were merged by condition using samtools merge. Bedtools
713 genomecov was run to convert the merged bam files into a bedgraph files. Finally,
714 bedGraphToBigWig (ucsc-tools/363) was used to generate the bigwig files displayed on
715 browser tracks using the IGV browser and compared to existing encode ATAC and
716 Chip-Seq peaks.
717

718 *scRNA-seq*

719 Fastq files were gathered from GEO from datasets GSE139088 GSE201653 and initial
720 counts were obtained using the Cell Ranger pipeline^{48,72}. Using Seurat v4, individual
721 cells were removed from the data set if they had fewer than 1000 discovered
722 genes/features, fewer than 1000 UMI or greater than 10% reads mapping to
723 mitochondrial genes. 2000 variable genes were found for each normalized library, and
724 anchors were selected for integration with dimensionality of each dataset set at 30. Glial
725 cells noted for the markers of *Sparc* and *Mpz* and non-neuronal cells lacking the
726 expression of *Avil* were excluded. Variable genes were identified from the merged
727 dataset, and PCA and UMAP were ran to generate new UMAP coordinates with a
728 dimensionality of 30 and clustering was performed with a resolution of 0.5.
729 Findallmarkers function utilizing a Wilcoxon rank-sum test was used to find cluster
730 specific markers and annotation was performed as recently established⁴⁸. Number of
731 *Oprd1* expressing cells were defined by a threshold of non-zero expression.
732

733 **Statistical analysis**

734 Statistical analysis was performed using GraphPad Prism 9 software. Data are
735 presented as mean \pm SEM. Differences pre- and post-injection within a single group

736 were assessed using a Wilcoxon matched-pairs signed rank test. Differences between
737 two groups were assessed using a Mann-Whitney test. Statistical analysis for multiple
738 comparisons were performed using Kruskal-Wallis test followed by Dunn's multiple
739 comparison test or a Two-Way ANOVA followed by Sidak's multiple comparison test.
740 $p < 0.05$ (*), $p < 0.01$ (**), $p < 0.001$ (***)
741

742 **Acknowledgement:** We thank Dr. Dena Dubal and her laboratory for the FCG mouse,
743 Dr. Kevin Yackle for *Penk*^{Cre} mice, Dr. Ari Molofsky for *Foxp3*^{Cre-ERT2}*Rosa26*^{TdTomato}
744 mice, Dr. Amynah Pradhan for *Oprd1*^{eGFP} mice and Dr. Mike Ansonoff for assistance
745 with *Penk*^{-/-} tissue isolation. We thank additional members of the Basbaum laboratory
746 and UCSF ImmunoX for critical feedback. Funding for this work was supported by
747 grants Canadian Institute of Health Research (CIHR) (to É.M.), the Fonds de Recherche
748 en Santé-Québec (to É.M.), the Dermatology Foundation (Career Development Award
749 to S.W.K.), the Sandler Foundation PBBR (to S.W.K.), Grunfeld Scholar Award from
750 SFVAMC (to S.W.K.), T32AR007175-44 (to S.W.K.), NIH NSR35NS097306 (to A.I.B.)
751 and Open Philanthropy (to A.I.B.). Figures were generated with BioRender.com.
752

753 **Disclosures:** Authors have no conflicts of interests to declare.
754

755 **Author contributions:** É.M. and S.W.K. designed experiments. É.M., B.C.M, J.B.,
756 S.R. N.P.K. W.L.E. and S.W.K. performed experiments, data analysis or visualization.
757 J.E.P. and A.I.D. provided critical reagents or tools. S.W.K, É.M. and A.I.B., acquired
758 funding and provided supervision. É.M, A.I.B and S.W.K. wrote the manuscript.
759

760 **Material availability and requests:** No new reagents, original code or original genomic
761 datasets were generated. Requests for reagents or mice can be sent to
762 sakeen.kashem@ucsf.edu or allan.basbaum@ucsf.edu.
763

764 **Diversity, equity, and inclusion statement:** Authors support diversity and inclusion
765 values. At least one author, including the lead author, self-identifies as a woman. At
766 least one author identifies as an under-represented minority and/or as an immigrant.
767
768
769
770
771
772
773
774
775
776
777
778
779
780
781

782 **Figure Legends**

783

784 **Figure 1. mTreg suppress mechanical pain hypersensitivity in female mice.**

785 Representative whole mount maximum projection confocal microscopy image of the (A)
786 lumbar spinal cord meninges and (B) DRG showing Tregs (green-red: yellow) and
787 nerves (autofluorescence, red) in *Foxp3*^{eGFP-CreERT2}; *Rosa26*^{tdTomato} reporter mice. Inlet
788 showing DRG magnification. Scale bar represents 100 μ m in A) and 150 μ m in B).
789 Arrows indicate Tregs. (C) Total number of weight-adjusted tissue Tregs across organs,
790 in both sexes combined. (D) Relative number of tissue Tregs from male (white) and
791 female (black) mice per organ. 100% represents mean number of female Tregs per
792 organ. Comparison is made between each individual organ. (E) Representative
793 concatenated flow cytometry plots of tissue Treg after a single intrathecal (IT) injection
794 of 20 ng of pegylated diphtheria toxin (pegDT). (F) Relative quantifications of tissue
795 Treg depletion 2 days after a single IT pegDT injection across organs. 100% represents
796 mean number of tissue Tregs in IT vehicle-injected mice per organ. (G and H) 50% paw
797 withdrawal thresholds measured using von Frey filaments before (day 0) and after a
798 single dose of 20 ng of IT pegDT or vehicle in female (G) or male (H) *Foxp3*-DTR mice.
799 (I) Summary of significant behavioral differences comparing IT pegDT- and control-
800 injected female and male mice. Total number of mice for G-I is presented in Figure S3.
801 ScMg= Spinal cord meninges, BrMg= Brain meninges, LN= Lymph nodes, ns = not
802 significant, * $p<0.05$, ** $p<0.01$, *** $p<0.001$. **Related to Figure S1-S3.**

803

804 **Figure 2. Expanding mTreg alleviates nociception dependent on sex hormones
805 and independent of tissue repair.**

806 (A) Schematic representation of the spared nerve injury (SNI) surgery. (B) Long-term
807 assessment of mechanical thresholds in mice following SNI surgery (both sexes
808 combined, no difference between the sexes). n = 7-8 mice per group. (C and D) Percent
809 response to 0.008 g von Frey filament in mice with SNI (day 0) and treated with IT
810 pegDT or vehicle every 4 days. n = 8 per group for females and 9-10 per group for
811 males. (E) Schematic representation of mTreg expansion in mice 4 weeks after SNI by
812 3 IT injections of low-dose IL-2 (0.1 μ g). (F) Total mTreg number in meninges after low-
813 dose IL-2 or vehicle IT injections (both sexes combined, no differences between the
814 sexes). (G and H) Nociceptive thresholds of females (G) and male (H) mice given low-
815 dose IL-2 or vehicle IT 4 weeks after SNI. (I) Schematic representation of the mating
816 strategy of Four Core Genotypes (FCG) *FoxP3*-DTR mice demonstrating resulting XX
817 and XY females and XX and XY male mice. (J and K) Nociceptive thresholds of FCG
818 female (J) and male (K) mice following low-dose IL-2 or vehicle IT injections 4 weeks
819 after SNI. (L) Anti-nociceptive efficacy determined as post IL-2/vehicle injection
820 threshold divided by baseline mechanical threshold in male and female mice with XX
821 (white) or XY (pink) chromosomes. (M) Nociceptive thresholds of FCG *FoxP3*-DTR
822 female and male mice following a single IT pegDT or vehicle injection. (N) Percent
823 baseline nociceptive thresholds determined as post pegDT/vehicle injection threshold
824 divided by baseline mechanical threshold in male and female mice with XX (white) or
825 XY (pink) chromosomes. ns = not significant, * $p<0.05$, ** $p<0.01$, *** $p<0.001$. **Related to
826 Figure S4.**

827

828 **Figure 3. mTregs express and produce enkephalin.**
829 (A) Volcano plot of transcription fold change of activated Treg (aTreg) vs resting Treg
830 (rTreg) and (B) heatmap of relative log2 expression value of aTreg, rTreg and activated
831 and resting CD4⁺ CD25⁻ conventional T cells (aTconv and rTconv) from public dataset
832 GSE154680 (n=3). (C) Averaged ATAC sequencing (ATACseq) of open chromatin
833 accessibility peaks on the *Penk* locus in different T cell subsets (n=4 per group,
834 GSE154680), compared to ATACseq, and histone modification Chip-Seq from public
835 ENCODE dataset of the p0 developing forebrain, a known enkephalinergic region. (D
836 and E) Log2 values of *Penk* expression by different unstimulated immune cell types
837 from Immgen dataset GSE180020. (E) Treg *Penk* expression fold change after cytokine
838 stimulation compared to vehicle control. (F) Representative PMA:Ionomycin stimulated
839 mTregs, meningeal CD4⁺ T cells (mCD4) from WT mice or *Penk*^{-/-} mTreg (control). (G)
840 Representative flow cytometry plots of Tregs from meninges or secondary lymphoid
841 organs (SLO) from *Penk*^{Cre}*Rosa26*^{tdTomato} mice. Pink represents non-vascular, tissue
842 Tregs from transgenic *Penk* lineage reporter mice. Gray represents vascular Treg in
843 reporter mice while Blue corresponds to tissue Treg from non-transgenic control mice.
844 (H-I) Number of enkephalin lineage fate reporter positive tissue Tregs in (H) meninges
845 and (I) secondary lymphoid organs (SLO) in male and female mice. NK: Natural Killer
846 cells, Tgd: $\gamma\delta$ T cells, Mo: Monocytes, MF.rp: Red pulp macrophages, CD4T: CD4⁺ T
847 cells, CD8T: CD8⁺ T cells, B.fo: splenic follicular B cells, DC8: CD8⁺ dendritic cells,
848 pDC: splenic plasmacytoid, MF.pc: peritoneal macrophages, MC: myeloid cells, B.mz:
849 splenic marginal zone B cells, ns = not significant, *p<0.05, **p<0.01, ***p<0.001.
850

851 **Figure 4. mTreg-derived enkephalin controls nociceptive thresholds.**
852 (A) Representative flow cytometry plots of Cre positive (pink) or Cre negative (blue)
853 CD45⁺ non-vascular cells from the meninges and the DRG, combined, from
854 *Penk*^{Cre}*Rosa26*^{tdTomato} mice. (B) Flow plot shows representative tdTomato negative and
855 right plot shows tdTomato positive leukocytes, demonstrating the more pronounced
856 mTreg representation in the enkephalinergic fate cell population. (C) Schematic
857 representation of bone marrow transplants to generate a global depletion of
858 enkephalinergic cells, a depletion of hematopoietic-derived enkephalin or a depletion of
859 Treg-derived enkephalin, respectively. (D-G) Bone marrow chimera of
860 *Penk*^{Cre}*Rosa26*^{DTR} → irradiated WT recipients. Nociceptive thresholds after a single
861 pegDT (pink) or vehicle (white) IT injection in female (D) and male (E) mice. n= 5 per
862 group. Nociceptive thresholds after SNI and pegDT (pink) or vehicle (white) IT injection
863 in female (F) and male (G) mice. (H) Nociceptive thresholds at baseline of female WT →
864 WT (black) or *Penk*^{-/-} → WT (white) bone marrow chimeras. (I) Female *Foxp3*-DTR +
865 *Penk*^{-/-} (1:1) → WT mice and tested for nociceptive thresholds after pegDT (pink) or
866 vehicle (white) IT, n=10 per group. (J) Nociceptive thresholds in SNI mice after pegDT
867 (pink) or vehicle (white) IT injections. (K) WT SNI female mice given low-dose IL-2 and
868 naltrindole. (L) Nociceptive efficacy calculated as percent compared to baseline
869 threshold. ns = not significant, *p<0.05, **p<0.01, ***p<0.001.
870
871
872
873

874 **Figure 5. Treg-derived enkephalin is dispensable for suppressing inflammation.**
875 (A) Baseline nociceptive thresholds of uninjured *Rag2*^{+/+, +/- or -/-} female mice. (B)
876 Nociceptive thresholds of female *Foxp3*-DTR mice injected with pegDT IT + IV
877 clodronate (pink) or control (white) liposomes showing peripheral macrophages do not
878 mediate the nociception induced by mTreg depletion, n=5 per group. (C) Representative
879 flow cytometry histograms of proliferated conventional T cells (Tconv) alone (pink) or
880 4:1 with WT Tregs (gray), *Penk*^{-/-} Tregs (yellow), or unstimulated, un-proliferated cell
881 trace violet-stained control (blue). Histogram shows cells that have not proliferated. (D)
882 Suppression of Tconv cell proliferation by different concentrations of WT Tregs (white)
883 or *Penk*^{-/-} Tregs (yellow). (E) Schematic representation of competition experiment
884 showing 1:1 transfer of WT or *Penk*^{-/-} T cells into *Rag2*^{-/-} mice. SNI surgery was
885 performed and organs were harvested 4 weeks later for F-H. (F) Equal competition of
886 *Penk* sufficient CD45.1 and *Penk* deficient CD45.2 CD4⁺ T cells in the meninges
887 represented as a concatenated flow cytometry plot, n=4 per group. Representative flow
888 cytometric plots. (G) Pooled proportion of *Penk* sufficient CD45.1 and *Penk* deficient
889 CD45.2 CD4⁺ T cells in different organs, n=4 per genotype. (H) Percent of FoxP3⁺, IFN-
890 \square ⁺ and IL-17A⁺ CD4⁺ T cells from G. (I) Representative flow cytometric plots of cytokine
891 secretion by CD4⁺ T cells after GVHD induced by transfer of pre-activated Tconv alone
892 or combined with *Penk*^{+/+} or *Penk*^{-/-} Tregs. (J) Weight curves of GVHD mice, n=3-4 per
893 group. ns = not significant, *p<0.05, **p<0.01, ***p<0.001. **Related to Figure S5.**
894

895 **Figure 6. δOR on MrgprD⁺ sensory neurons is required for mTreg mediated anti-**
896 **nociception.**

897 (A) Schematic representation of AAV-induced ablation of *Oprd1* in the PNS (B-C) or
898 CNS. (B) Nociceptive thresholds of female mice lacking *Oprd1* in the PNS after mTreg
899 expansion compared to controls. (C) Anti-nociceptive efficacy of mTreg expansion. (D)
900 No difference in nociceptive thresholds in female mice lacking *Oprd1* in the CNS after
901 mTreg expansion compared to controls. (E) Heatmap of row normalized expression
902 from DRG sensory neurons clusters from combined GSE139088 and GSE201653. (F)
903 Proportions of sensory neuron clusters expressing *Oprd1* from E. (G) Representative
904 flow cytometry plot of δOR-GFP (green) expression on IB4⁺ MrgprD⁺ DRG sensory
905 neurons compared to cells from non-reporter mice (purple). Overlaid are lymphoid
906 CD45⁺ CD90.2⁺ cells and myeloid CD45⁺ CD11b⁺ cells from the DRG. (H-I) Percent
907 response to 0.008 g von Frey fiber stimulation after SNI in female (H) or male (I) mice
908 conditionally lacking δOR on MrgprD⁺ neurons (pink) or controls (white). (J) Nociceptive
909 thresholds after mTreg expansion in female mice lacking *Oprd1* in MrgprD⁺ neurons
910 compared to controls. (K) Anti-nociceptive efficacy of mTreg expansion. SA-LTMR=
911 Slowly adapting low-threshold mechanoreceptor, RA-LTMR= rapidly-adapting low-
912 threshold mechanoreceptor, MrgprD= Mas-related G protein-coupled receptor D, Prop.=
913 proprioceptor, SST: somatostatin, Trpm8= Transient receptor potential cation channel
914 subfamily M member 8, TAM= Tamoxifen, cKO= Conditional KO, ns = not significant,
915 *p<0.05, **p<0.01, ***p<0.001.

916
917
918
919

920

921 Supplemental Figure Legends

922

923 **Figure S1. Flow cytometric gating strategy of meningeal Tregs.**

924 (A) Gating strategy to quantify tissue Treg numbers. Numbers indicate gate frequency.
925 Mice were injected IT with ARTC2 nanobody to minimize Treg apoptosis and injected IV
926 with anti-CD45 FITC (pink) antibody or vehicle injected (blue) to label vascular immune
927 cells.

928

929 **Figure S2. pegDT IT injection avoids systemic inflammation and weight loss in** 930 ***Foxp3*-DTR mice.**

931 (A) Evan's blue staining after IT injection showing diffusion into the cerebellum, the
932 olfactory bulb, the cervical and lumbar lymph nodes, the spinal cord meninges and the
933 lumbar DRG. (B) pegDyLight650 IT injection exhibits a more limited diffusion than
934 Evan's blue. (C) Weight curves of *Foxp3*-DTR mice injected with IT pegDT, IP DT or IT
935 vehicle every 3 days demonstrating a lack of weight loss after site-selective Treg
936 ablation. Arrows represent DT injections. (D and E) Representative images of spleen
937 sizes and spleen weights from mice in (C). (F) Survival curves of mice in (C). ns = not
938 significant, * $p<0.05$, ** $p<0.01$, *** $p<0.001$.

939

940 **Figure S3. mTreg depletion selectively induces mechanical hypersensitivity in** 941 **female mice.**

942 (A) von Frey, (B) Hargreaves, (C) hotplate, (D) tail flick, (E) acetone, (F) pinprick, (G)
943 brush and (G) rotarod behavioral testing in *FoxP3*-DTR mice injected with a single dose
944 of IT pegDT. n = 4-20 mice per group. ns = not significant, **** $p<0.0001$.

945

946 **Figure S4. mTreg expansion selectively improves mechanical hypersensitivity in** 947 **injured female mice.**

948 (A) mTreg expansion using IL-2 IT injections induces no changes in nociceptive
949 thresholds in uninjured naive male and female mice. mTreg expansion in nerve-injured
950 mice induces no changes in (B) acetone, (C) Hargreaves and (D) hotplate behavioral
951 testing. ns = not significant.

952

953 **Figure S5. Functional characterization of enkephalin from CD4⁺ T cells.**

954 (A) Chimerism of meningeal Tregs and spinal cord microglia in PenkDTR^{Δheme} mice and
955 (B) pooled chimerism comparing Tregs in the meninges and in the lymphoid organs
956 compared to tissue macrophages of the spinal cord (microglia) and the epidermis
957 (Langerhans cells, LC). (C) mTreg number after IP DT injection in PenkDTR^{Δheme} mice.
958 (D) Weight curves of PenkDTR^{Δheme} mice injected with IP DT every three days showing
959 peripheral penk ablation doesn't induce weight loss. (E) Unaltered spleen weight and
960 (F) meningeal and (G) spleen CD4⁺ T cell populations after IP DT. Unaltered CD4 T cell
961 populations in the (H) spleen and (I) in the nerve and unaltered (J) mouse weight and
962 (K) spleen weight. (L) Graft Versus Host Disease (GVHD) score in *Rag2*^{-/-} mice injected
963 with pre-activated Tconv alone or with *Penk*^{+/+} or *Penk*^{-/-} Tregs, n=3-4 mice per group.
964 (M) IFN- \square ⁺ and (N) IL-17⁺ CD4⁺ T cells after GVHD induction. ns = not significant,
965 * $p<0.05$, *** $p<0.001$.

966

References

1. Mogil, J.S. (2012). Sex differences in pain and pain inhibition: multiple explanations of a controversial phenomenon. *Nat. Rev. Neurosci.* *13*, 859–866. [10.1038/nrn3360](https://doi.org/10.1038/nrn3360).
2. Aloisi, A.M., Bachiocco, V., Costantino, A., Stefani, R., Ceccarelli, I., Bertaccini, A., and Merigliola, M.C. (2007). Cross-sex hormone administration changes pain in transsexual women and men. *Pain* *132 Suppl 1*, S60–S67. [10.1016/j.pain.2007.02.006](https://doi.org/10.1016/j.pain.2007.02.006).
3. Petrovski, B.É., Vetvik, K.G., Lundqvist, C., and Eberhard-Gran, M. (2018). Characteristics of menstrual versus non-menstrual migraine during pregnancy: a longitudinal population-based study. *J. Headache Pain* *19*, 27. [10.1186/s10194-018-0853-3](https://doi.org/10.1186/s10194-018-0853-3).
4. Negro, A., Delaruelle, Z., Ivanova, T.A., Khan, S., Ornello, R., Raffaelli, B., Terrin, A., Reuter, U., Mitsikostas, D.D., and European Headache Federation School of Advanced Studies (EHF-SAS) (2017). Headache and pregnancy: a systematic review. *J. Headache Pain* *18*, 106. [10.1186/s10194-017-0816-0](https://doi.org/10.1186/s10194-017-0816-0).
5. Melhado, E.M., Maciel, J.A., and Guerreiro, C.A.M. (2007). Headache during gestation: evaluation of 1101 women. *Can. J. Neurol. Sci. J. Can. Sci. Neurol.* *34*, 187–192. [10.1017/s0317167100006028](https://doi.org/10.1017/s0317167100006028).
6. Gintzler, A.R. (1980). Endorphin-Mediated Increases in Pain Threshold During Pregnancy. *Science* *210*, 193–195. [10.1126/science.7414330](https://doi.org/10.1126/science.7414330).
7. Ray-Griffith, S.L., Wendel, M.P., Stowe, Z.N., and Magann, E.F. (2018). Chronic pain during pregnancy: a review of the literature. *Int. J. Womens Health* *10*, 153–164. [10.2147/IJWH.S151845](https://doi.org/10.2147/IJWH.S151845).
8. Burzyn, D., Kuswanto, W., Kolodin, D., Shadrach, J.L., Cerletti, M., Jang, Y., Sefik, E., Tan, T.G., Wagers, A.J., Benoist, C., et al. (2013). A Special Population of Regulatory T Cells Potentiates Muscle Repair. *Cell* *155*, 1282–1295. [10.1016/j.cell.2013.10.054](https://doi.org/10.1016/j.cell.2013.10.054).
9. Astarita, J.L., Dominguez, C.X., Tan, C., Guillen, J., Pauli, M.L., Labastida, R., Valle, J., Kleinschek, M., Lyons, J., and Zarrin, A.A. (2023). Treg specialization and functions beyond immune suppression. *Clin. Exp. Immunol.* *211*, 176–183. [10.1093/cei/uxac123](https://doi.org/10.1093/cei/uxac123).
10. Samstein, R.M., Josefowicz, S.Z., Arvey, A., Treuting, P.M., and Rudensky, A.Y. (2012). Extrathymic generation of regulatory T cells in placental mammals mitigates maternal-fetal conflict. *Cell* *150*, 29–38. [10.1016/j.cell.2012.05.031](https://doi.org/10.1016/j.cell.2012.05.031).
11. Arpaia, N., Green, J.A., Moltedo, B., Arvey, A., Hemmers, S., Yuan, S., Treuting, P.M., and Rudensky, A.Y. (2015). A Distinct Function of Regulatory T Cells in Tissue Protection. *Cell* *162*, 1078–1089. [10.1016/j.cell.2015.08.021](https://doi.org/10.1016/j.cell.2015.08.021).

12. Ali, N., Zirak, B., Rodriguez, R.S., Pauli, M.L., Truong, H.-A., Lai, K., Ahn, R., Corbin, K., Lowe, M.M., Scharschmidt, T.C., et al. (2017). Regulatory T Cells in Skin Facilitate Epithelial Stem Cell Differentiation. *Cell* **169**, 1119–1129.e11. [10.1016/j.cell.2017.05.002](https://doi.org/10.1016/j.cell.2017.05.002).
13. Bapat, S.P., Myoung Suh, J., Fang, S., Liu, S., Zhang, Y., Cheng, A., Zhou, C., Liang, Y., LeBlanc, M., Liddle, C., et al. (2015). Depletion of fat-resident Treg cells prevents age-associated insulin resistance. *Nature* **528**, 137–141. [10.1038/nature16151](https://doi.org/10.1038/nature16151).
14. Salvany-Celades, M., Van Der Zwan, A., Benner, M., Setrajcic-Dragos, V., Bougleux Gomes, H.A., Iyer, V., Norwitz, E.R., Strominger, J.L., and Tilburgs, T. (2019). Three Types of Functional Regulatory T Cells Control T Cell Responses at the Human Maternal-Fetal Interface. *Cell Rep.* **27**, 2537–2547.e5. [10.1016/j.celrep.2019.04.109](https://doi.org/10.1016/j.celrep.2019.04.109).
15. Robertson, S.A., Care, A.S., and Moldenhauer, L.M. (2018). Regulatory T cells in embryo implantation and the immune response to pregnancy. *J. Clin. Invest.* **128**, 4224–4235. [10.1172/JCI122182](https://doi.org/10.1172/JCI122182).
16. Rowe, J.H., Ertelt, J.M., Xin, L., and Way, S.S. (2012). Pregnancy imprints regulatory memory that sustains anergy to fetal antigen. *Nature* **490**, 102–106. [10.1038/nature11462](https://doi.org/10.1038/nature11462).
17. Davoli-Ferreira, M., de Lima, K.A., Fonseca, M.M., Guimarães, R.M., Gomes, F.I., Cavallini, M.C., Quadros, A.U., Kusuda, R., Cunha, F.Q., Alves-Filho, J.C., et al. (2020). Regulatory T cells counteract neuropathic pain through inhibition of the Th1 response at the site of peripheral nerve injury. *Pain* **161**, 1730–1743. [10.1097/j.pain.0000000000001879](https://doi.org/10.1097/j.pain.0000000000001879).
18. Kuhn, J.A., Vainchtein, I.D., Braz, J., Hamel, K., Bernstein, M., Craik, V., Dahlgren, M.W., Ortiz-Carpena, J., Molofsky, A.B., Molofsky, A.V., et al. (2021). Regulatory T-cells inhibit microglia-induced pain hypersensitivity in female mice. *eLife* **10**, e69056. [10.7554/eLife.69056](https://doi.org/10.7554/eLife.69056).
19. Ito, M., Komai, K., Mise-Omata, S., Iizuka-Koga, M., Noguchi, Y., Kondo, T., Sakai, R., Matsuo, K., Nakayama, T., Yoshie, O., et al. (2019). Brain regulatory T cells suppress astrogliosis and potentiate neurological recovery. *Nature* **565**, 246–250. [10.1038/s41586-018-0824-5](https://doi.org/10.1038/s41586-018-0824-5).
20. Dombrowski, Y., O'Hagan, T., Dittmer, M., Penalva, R., Mayoral, S.R., Bankhead, P., Fleville, S., Eleftheriadis, G., Zhao, C., Naughton, M., et al. (2017). Regulatory T cells promote myelin regeneration in the central nervous system. *Nat. Neurosci.* **20**, 674–680. [10.1038/nn.4528](https://doi.org/10.1038/nn.4528).
21. Scherrer, G., Imamachi, N., Cao, Y.-Q., Contet, C., Mennicken, F., O'Donnell, D., Kieffer, B.L., and Basbaum, A.I. (2009). Dissociation of the opioid receptor mechanisms that control mechanical and heat pain. *Cell* **137**, 1148–1159. [10.1016/j.cell.2009.04.019](https://doi.org/10.1016/j.cell.2009.04.019).
22. François, A., Low, S.A., Sypek, E.I., Christensen, A.J., Sotoudeh, C., Beier, K.T., Ramakrishnan, C., Ritola, K.D., Sharif-Naeini, R., Deisseroth, K., et al. (2017). A Brainstem-Spinal Cord Inhibitory Circuit for Mechanical Pain Modulation by GABA and Enkephalins. *Neuron* **93**, 822–839.e6. [10.1016/j.neuron.2017.01.008](https://doi.org/10.1016/j.neuron.2017.01.008).

23. Wang, D., Tawfik, V.L., Corder, G., Low, S.A., François, A., Basbaum, A.I., and Scherrer, G. (2018). Functional Divergence of Delta and Mu Opioid Receptor Organization in CNS Pain Circuits. *Neuron* **98**, 90-108.e5. [10.1016/j.neuron.2018.03.002](https://doi.org/10.1016/j.neuron.2018.03.002).
24. Sorge, R.E., Mapplebeck, J.C.S., Rosen, S., Beggs, S., Taves, S., Alexander, J.K., Martin, L.J., Austin, J.-S., Sotocinal, S.G., Chen, D., et al. (2015). Different immune cells mediate mechanical pain hypersensitivity in male and female mice. *Nat. Neurosci.* **18**, 1081–1083. [10.1038/nn.4053](https://doi.org/10.1038/nn.4053).
25. Othy, S., Jairaman, A., Dynes, J.L., Dong, T.X., Tune, C., Yeromin, A.V., Zavala, A., Akunwafo, C., Chen, F., Parker, I., et al. (2020). Regulatory T cells suppress Th17 cell Ca²⁺ signaling in the spinal cord during murine autoimmune neuroinflammation. *Proc. Natl. Acad. Sci.* **117**, 20088–20099. [10.1073/pnas.2006895117](https://doi.org/10.1073/pnas.2006895117).
26. Maganin, A.G., Souza, G.R., Fonseca, M.D., Lopes, A.H., Guimarães, R.M., Dagostin, A., Cecilio, N.T., Mendes, A.S., Gonçalves, W.A., Silva, C.E.A., et al. (2022). Meningeal dendritic cells drive neuropathic pain through elevation of the kynurenone metabolic pathway in mice. *J. Clin. Invest.* **132**. [10.1172/JCI153805](https://doi.org/10.1172/JCI153805).
27. Anderson, K.G., Mayer-Barber, K., Sung, H., Beura, L., James, B.R., Taylor, J.J., Qunaj, L., Griffith, T.S., Vezys, V., Barber, D.L., et al. (2014). Intravascular staining for discrimination of vascular and tissue leukocytes. *Nat. Protoc.* **9**, 209–222. [10.1038/nprot.2014.005](https://doi.org/10.1038/nprot.2014.005).
28. Pereira, M.M.A., Mahú, I., Seixas, E., Martínez-Sánchez, N., Kubasova, N., Pirzgalska, R.M., Cohen, P., Dietrich, M.O., López, M., Bernardes, G.J.L., et al. (2017). A brain-sparing diphtheria toxin for chemical genetic ablation of peripheral cell lineages. *Nat. Commun.* **8**, 14967. [10.1038/ncomms14967](https://doi.org/10.1038/ncomms14967).
29. Minarelli, J., Davis, E.L., Dickerson, A., Moore, W.C., Mejia, J.A., Gugala, Z., Olmsted-Davis, E.A., and Davis, A.R. (2019). Characterization of neuromas in peripheral nerves and their effects on heterotopic bone formation. *Mol. Pain* **15**, 1744806919838191. [10.1177/1744806919838191](https://doi.org/10.1177/1744806919838191).
30. Xie, W., Strong, J.A., and Zhang, J.-M. (2017). Active Nerve Regeneration with Failed Target Reinnervation Drives Persistent Neuropathic Pain. *eNeuro* **4**. [10.1523/ENEURO.0008-17.2017](https://doi.org/10.1523/ENEURO.0008-17.2017).
31. Graßhoff, H., Comdühr, S., Monne, L.R., Müller, A., Lamprecht, P., Riemekasten, G., and Humrich, J.Y. (2021). Low-Dose IL-2 Therapy in Autoimmune and Rheumatic Diseases. *Front. Immunol.* **12**, 648408. [10.3389/fimmu.2021.648408](https://doi.org/10.3389/fimmu.2021.648408).
32. Syrett, C.M., Paneru, B., Sandoval-Heglund, D., Wang, J., Banerjee, S., Sindhava, V., Behrens, E.M., Atchison, M., and Anguera, M.C. (2019). Altered X-chromosome inactivation in T cells may promote sex-biased autoimmune diseases. *JCI Insight* **4**. [10.1172/jci.insight.126751](https://doi.org/10.1172/jci.insight.126751).

33. Pyfrom, S., Paneru, B., Knox, J.J., Cancro, M.P., Posso, S., Buckner, J.H., and Anguera, M.C. (2021). The dynamic epigenetic regulation of the inactive X chromosome in healthy human B cells is dysregulated in lupus patients. *Proc. Natl. Acad. Sci. U. S. A.* **118**, e2024624118. [10.1073/pnas.2024624118](https://doi.org/10.1073/pnas.2024624118).
34. Jiwrajka, N., Toothacre, N.E., Beethem, Z.T., Sting, S., Forsyth, K.S., Dubin, A.H., Driscoll, A., Stohl, W., and Anguera, M.C. (2023). Impaired dynamic X-chromosome inactivation maintenance in T cells is a feature of spontaneous murine SLE that is exacerbated in female-biased models. *J. Autoimmun.* **139**, 103084. [10.1016/j.jaut.2023.103084](https://doi.org/10.1016/j.jaut.2023.103084).
35. Arnold, A.P. (2020). Four Core Genotypes and XY* mouse models: Update on impact on SABV research. *Neurosci. Biobehav. Rev.* **119**, 1–8. [10.1016/j.neubiorev.2020.09.021](https://doi.org/10.1016/j.neubiorev.2020.09.021).
36. Arnold, A.P., and Chen, X. (2009). What does the “four core genotypes” mouse model tell us about sex differences in the brain and other tissues? *Front. Neuroendocrinol.* **30**, 1–9. [10.1016/j.yfrne.2008.11.001](https://doi.org/10.1016/j.yfrne.2008.11.001).
37. Shime, H., Odanaka, M., Tsuiji, M., Matoba, T., Imai, M., Yasumizu, Y., Uraki, R., Minohara, K., Watanabe, M., Bonito, A.J., et al. (2020). Proenkephalin+ regulatory T cells expanded by ultraviolet B exposure maintain skin homeostasis with a healing function. *Proc. Natl. Acad. Sci.* **117**, 20696–20705. [10.1073/pnas.2000372117](https://doi.org/10.1073/pnas.2000372117).
38. Galván-Peña, S., Leon, J., Chowdhary, K., Michelson, D.A., Vijaykumar, B., Yang, L., Magnuson, A.M., Chen, F., Manickas-Hill, Z., Piechocka-Trocha, A., et al. (2021). Profound Treg perturbations correlate with COVID-19 severity. *Proc. Natl. Acad. Sci.* **118**, e2111315118. [10.1073/pnas.2111315118](https://doi.org/10.1073/pnas.2111315118).
39. Sjaastad, L.E., Owen, D.L., Joo, S., Knutson, T.P., O'Connor, C.H., McCluskey, B., LaRue, R.S., Langlois, R.A., and Farrar, M.A. (2022). Influenza infection recruits distinct waves of regulatory T cells to the lung that limit lung resident IgA+ B cells. Preprint at bioRxiv, [10.1101/2022.09.19.508325](https://doi.org/10.1101/2022.09.19.508325) [10.1101/2022.09.19.508325](https://doi.org/10.1101/2022.09.19.508325).
40. van der Veeken, J., Glasner, A., Zhong, Y., Hu, W., Wang, Z.-M., Bou-Puerto, R., Charbonnier, L.-M., Chatila, T.A., Leslie, C.S., and Rudensky, A.Y. (2020). The transcription factor Foxp3 shapes regulatory T cell identity by tuning the activity of trans-acting intermediaries. *Immunity* **53**, 971–984.e5. [10.1016/j.immuni.2020.10.010](https://doi.org/10.1016/j.immuni.2020.10.010).
41. Gong, S., Zheng, C., Doughty, M.L., Losos, K., Didkovsky, N., Schambra, U.B., Nowak, N.J., Joyner, A., Leblanc, G., Hatten, M.E., et al. (2003). A gene expression atlas of the central nervous system based on bacterial artificial chromosomes. *Nature* **425**, 917–925. [10.1038/nature02033](https://doi.org/10.1038/nature02033).
42. Baysoy, A., Seddu, K., Salloum, T., Dawson, C.A., Lee, J.J., Yang, L., Gal-oz, S., Ner-Gaon, H., Tellier, J., Millan, A., et al. (2023). The interweaved signatures of common-gamma-chain

cytokines across immunologic lineages. *J. Exp. Med.* **220**, e20222052. 10.1084/jem.20222052.

43. Zamir, N., Palkovits, M., Weber, E., Mezey, E., and Brownstein, M.J. (1984). A dynorphinergic pathway of Leu-enkephalin production in rat substantia nigra. *Nature* **307**, 643–645. 10.1038/307643a0.

44. Cugurra, A., Mamuladze, T., Rustenhoven, J., Dykstra, T., Beroshvili, G., Greenberg, Z.J., Baker, W., Papadopoulos, Z., Drieu, A., Blackburn, S., et al. (2021). Skull and vertebral bone marrow are myeloid cell reservoirs for the meninges and CNS parenchyma. *Science* **373**, eabf7844. 10.1126/science.abf7844.

45. Weisser, S.B., van Rooijen, N., and Sly, L.M. (2012). Depletion and Reconstitution of Macrophages in Mice. *J. Vis. Exp. JoVE*, 4105. 10.3791/4105.

46. Sankaranarayanan, I., Tavares-Ferreira, D., Mwirigi, J.M., Mejia, G.L., Burton, M.D., and Price, T.J. (2023). Inducible co-stimulatory molecule (ICOS) alleviates paclitaxel-induced neuropathic pain via an IL-10-mediated mechanism in female mice. *J. Neuroinflammation* **20**. 10.1186/s12974-023-02719-8.

47. Laumet, G., Bavencoffe, A., Edralin, J.D., Huo, X.-J., Walters, E.T., Dantzer, R., Heijnen, C.J., and Kavelaars, A. (2020). Interleukin-10 resolves pain hypersensitivity induced by cisplatin by reversing sensory neuron hyperexcitability. *PAIN* **161**, 2344. 10.1097/j.pain.0000000000001921.

48. Qi, L., Iskols, M., Shi, D., Reddy, P., Walker, C., Lezgiyeva, K., Voisin, T., Pawlak, M., Kuchroo, V.K., Chiu, I.M., et al. (2024). A mouse DRG genetic toolkit reveals morphological and physiological diversity of somatosensory neuron subtypes. *Cell* **187**, 1508-1526.e16. 10.1016/j.cell.2024.02.006.

49. Rosen, S.F., Ham, B., Drouin, S., Boachie, N., Chabot-Dore, A.-J., Austin, J.-S., Diatchenko, L., and Mogil, J.S. (2017). T-Cell Mediation of Pregnancy Analgesia Affecting Chronic Pain in Mice. *J. Neurosci. Off. J. Soc. Neurosci.* **37**, 9819–9827. 10.1523/JNEUROSCI.2053-17.2017.

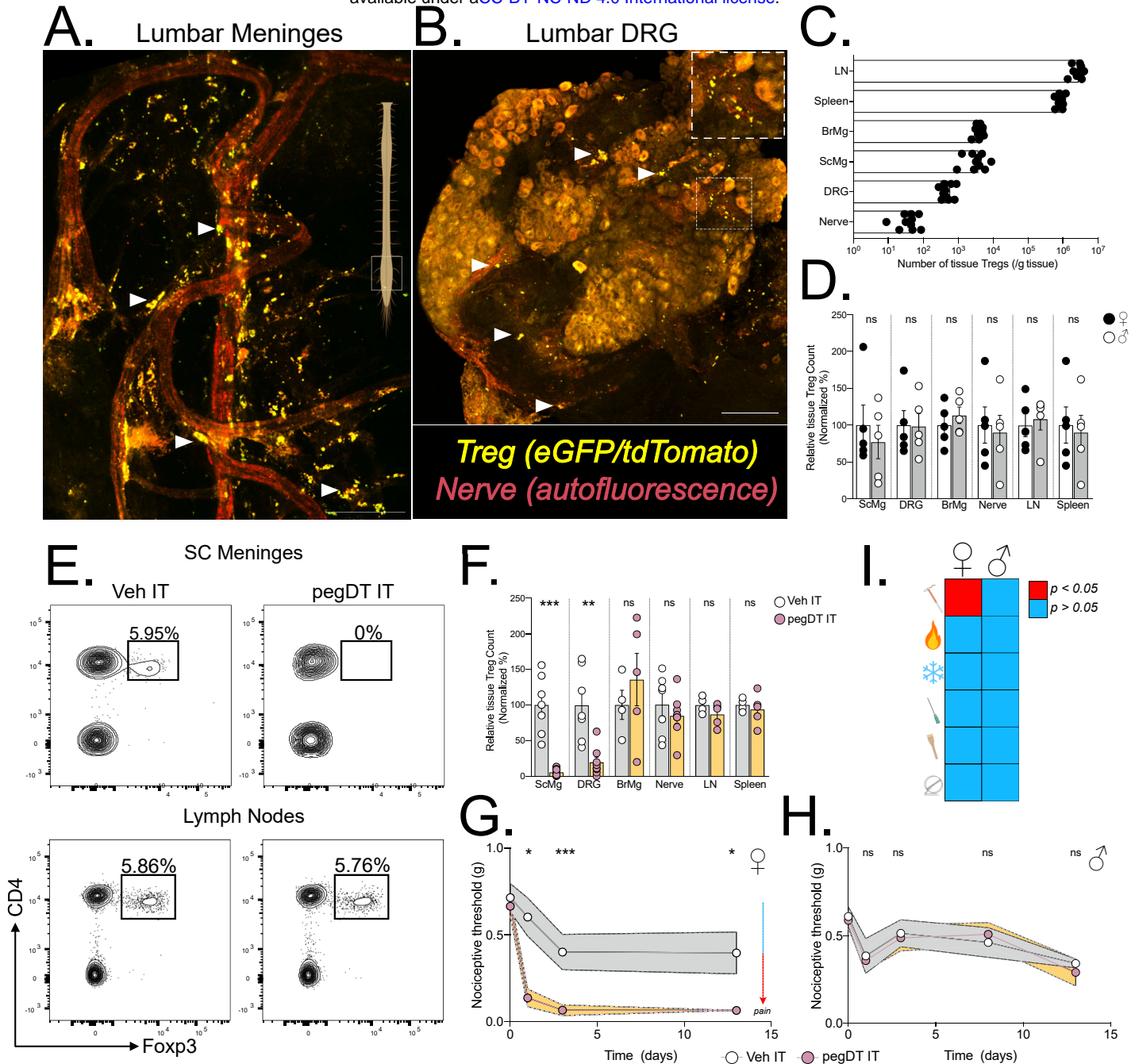
50. Baron, S.A., and Gintzler, A.R. (1984). Pregnancy-induced analgesia: effects of adrenalectomy and glucocorticoid replacement. *Brain Res.* **321**, 341–346. 10.1016/0006-8993(84)90190-2.

51. Munoz-Suano, A., Kallikourdis, M., Sarris, M., and Betz, A.G. (2012). Regulatory T cells protect from autoimmune arthritis during pregnancy. *J. Autoimmun.* **38**, J103–J108. 10.1016/j.jaut.2011.09.007.

52. Barry, A.M., Zhao, N., Yang, X., Bennett, D.L., and Baskozos, G. (2023). Deep RNA-seq of male and female murine sensory neuron subtypes after nerve injury. *PAIN* **164**, 2196. 10.1097/j.pain.0000000000002934.

53. Midavaine, É., Côté, J., Marchand, S., and Sarret, P. (2021). Glial and neuroimmune cell choreography in sexually dimorphic pain signaling. *Neurosci. Biobehav. Rev.* *125*, 168–192. 10.1016/j.neubiorev.2021.01.023.
54. van Rooijen, D.E., Roelen, D.L., Verduijn, W., Haasnoot, G.W., Huygen, F.J.P.M., Perez, R.S.G.M., Claas, F.H.J., Marinus, J., van Hilt, J.J., and van den Maagdenberg, A.M.J.M. (2012). Genetic HLA Associations in Complex Regional Pain Syndrome With and Without Dystonia. *J. Pain* *13*, 784–789. 10.1016/j.jpain.2012.05.003.
55. Aubert, N., Purcarea, M., Fornier, M., Cagnet, L., Naturel, M., Casrouge, A., Dietrich, G., Dieu-Nosjean, M.-C., and Marodon, G. (2024). Enkephalin-mediated modulation of basal somatic sensitivity by regulatory T cells in mice. *eLife* *13*. 10.7554/eLife.91359.1.
56. R, B., VI, T., D, W., A, F., C, S., Sa, S., P, C., C, B., C, C., K, S., et al. (2014). Delta opioid receptors presynaptically regulate cutaneous mechanosensory neuron input to the spinal cord dorsal horn. *Neuron* *81*. 10.1016/j.neuron.2014.01.044.
57. G, S., Ta, A., F, S., C, S., G, S.-J., G, G., G, M., and H, S. (1988). Naloxone does not alter the perception of pain induced by electrical and thermal stimulation of the skin in healthy humans. *Pain* *34*. 10.1016/0304-3959(88)90122-4.
58. A, A., M, H., Al, H., O, H., and A, B. (1999). Estrogen-induced alterations of spinal cord enkephalin gene expression. *Pain* *83*. 10.1016/s0304-3959(99)00109-8.
59. Adurthi, S., Kumar, M.M., Vinodkumar, H.S., Mukherjee, G., Krishnamurthy, H., Acharya, K.K., Bafna, U.D., Uma, D.K., Abhishek, B., Krishna, S., et al. (2017). Oestrogen Receptor- α binds the FOXP3 promoter and modulates regulatory T-cell function in human cervical cancer. *Sci. Rep.* *7*, 17289. 10.1038/s41598-017-17102-w.
60. Nitsche, J.F., Schuller, A.G.P., King, M.A., Zengh, M., Pasternak, G.W., and Pintar, J.E. (2002). Genetic Dissociation of Opiate Tolerance and Physical Dependence in δ -Opioid Receptor-1 and Preproenkephalin Knock-Out Mice. *J. Neurosci.* *22*, 10906–10913. 10.1523/JNEUROSCI.22-24-10906.2002.
61. Pereira, M.M.A., Mahú, I., Seixas, E., Martínez-Sánchez, N., Kubasova, N., Pirzgalska, R.M., Cohen, P., Dietrich, M.O., López, M., Bernardes, G.J.L., et al. (2017). A brain-sparing diphtheria toxin for chemical genetic ablation of peripheral cell lineages. *Nat. Commun.* *8*, 14967. 10.1038/ncomms14967.
62. Sorge, R.E., Martin, L.J., Isbester, K.A., Sotocinal, S.G., Rosen, S., Tuttle, A.H., Wieskopf, J.S., Acland, E.L., Dokova, A., Kadoura, B., et al. (2014). Olfactory exposure to males, including men, causes stress and related analgesia in rodents. *Nat. Methods* *11*, 629–632. 10.1038/nmeth.2935.
63. Dixon, W.J. (1965). The Up-and-Down Method for Small Samples. *J. Am. Stat. Assoc.* *60*, 967–978. 10.2307/2283398.

64. Chaplan, S.R., Bach, F.W., Pogrel, J.W., Chung, J.M., and Yaksh, T.L. (1994). Quantitative assessment of tactile allodynia in the rat paw. *J. Neurosci. Methods* **53**, 55–63. 10.1016/0165-0270(94)90144-9.
65. Shields, S.D., Eckert, W.A., and Basbaum, A.I. (2003). Spared nerve injury model of neuropathic pain in the mouse: a behavioral and anatomic analysis. *J. Pain* **4**, 465–470. 10.1067/S1526-5900(03)00781-8.
66. Park, Y.-G., Sohn, C.H., Chen, R., McCue, M., Yun, D.H., Drummond, G.T., Ku, T., Evans, N.B., Oak, H.C., Trieu, W., et al. (2018). Protection of tissue physicochemical properties using polyfunctional crosslinkers. *Nat. Biotechnol.* 10.1038/nbt.4281.
67. Borges da Silva, H., Wang, H., Qian, L.J., Hogquist, K.A., and Jameson, S.C. (2019). ARTC2.2/P2RX7 Signaling during Cell Isolation Distorts Function and Quantification of Tissue-Resident CD8+ T Cell and Invariant NKT Subsets. *J. Immunol.* **202**, 2153–2163. 10.4049/jimmunol.1801613.
68. Heinen, A.P., Wanke, F., Moos, S., Attig, S., Luche, H., Pal, P.P., Budisa, N., Fehling, H.J., Waisman, A., and Kurschus, F.C. (2014). Improved method to retain cytosolic reporter protein fluorescence while staining for nuclear proteins. *Cytom. Part J. Int. Soc. Anal. Cytol.* **85**, 621–627. 10.1002/cyto.a.22451.
69. Collison, L.W., and Vignali, D.A.A. (2011). In Vitro Treg Suppression Assays. *Methods Mol. Biol.* Clifton NJ **707**, 21–37. 10.1007/978-1-61737-979-6_2.
70. Schroeder, M.A., and DiPersio, J.F. (2011). Mouse models of graft-versus-host disease: advances and limitations. *Dis. Model. Mech.* **4**, 318–333. 10.1242/dmm.006668.
71. Hess, N.J., Hudson, A.W., Hematti, P., and Gumperz, J.E. (2020). Early T Cell Activation Metrics Predict Graft-versus-Host Disease in a Humanized Mouse Model of Hematopoietic Stem Cell Transplantation. *J. Immunol.* **205**, 272–281. 10.4049/jimmunol.2000054.
72. N, S., K, F., K, L., De, W., Am, K., and Dd, G. (2020). The emergence of transcriptional identity in somatosensory neurons. *Nature* **577**. 10.1038/s41586-019-1900-1.



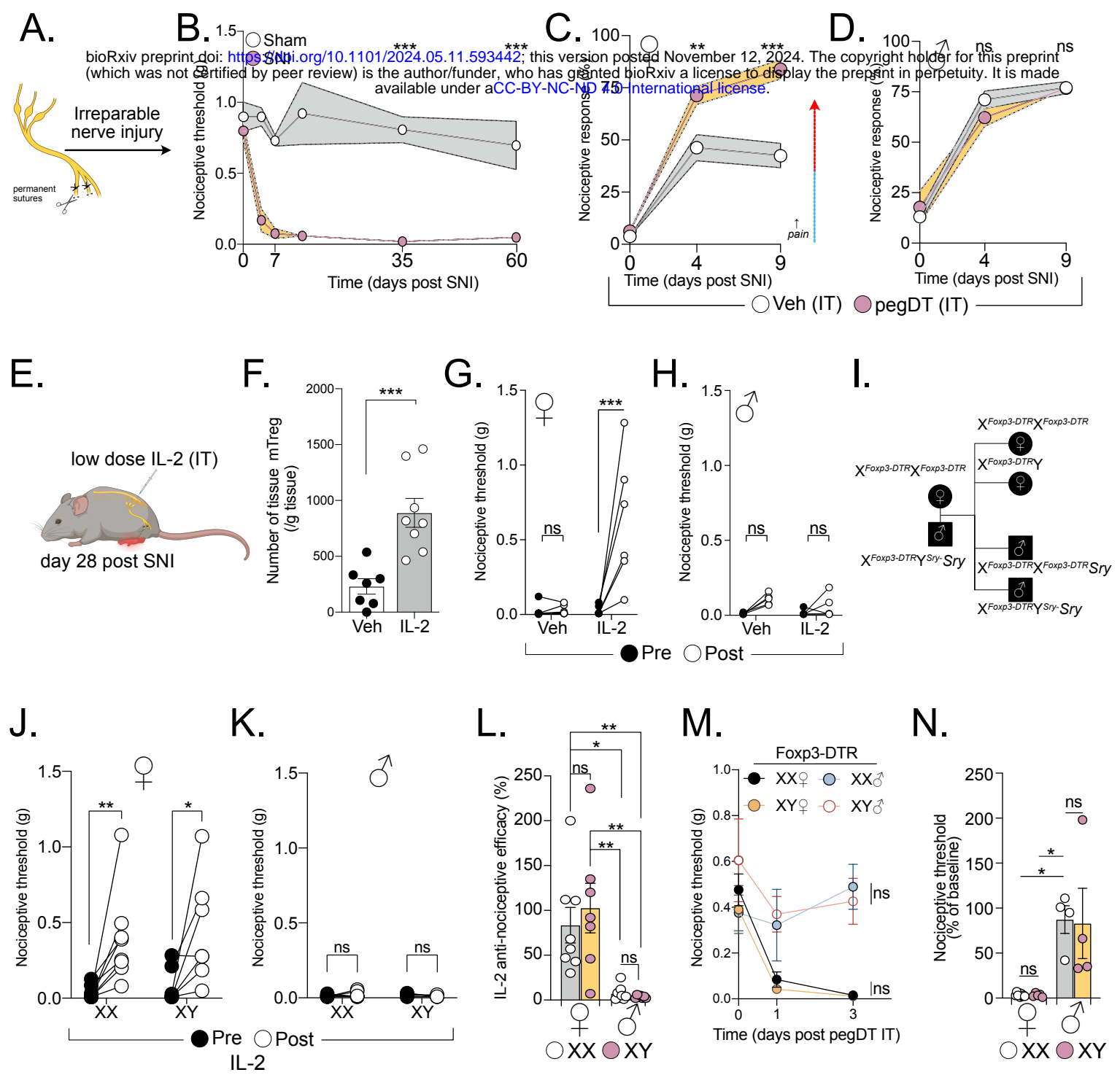
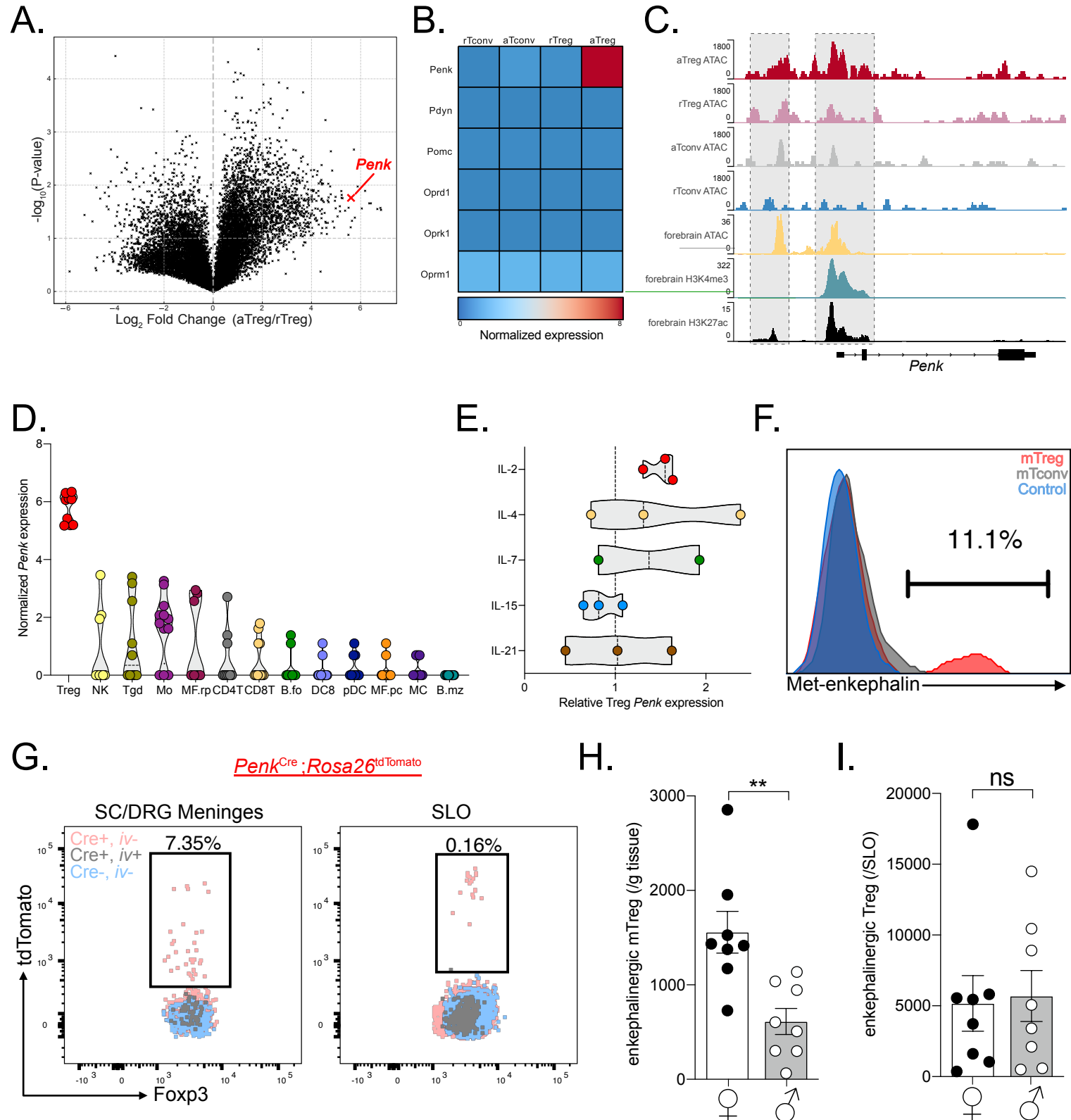


Figure 3



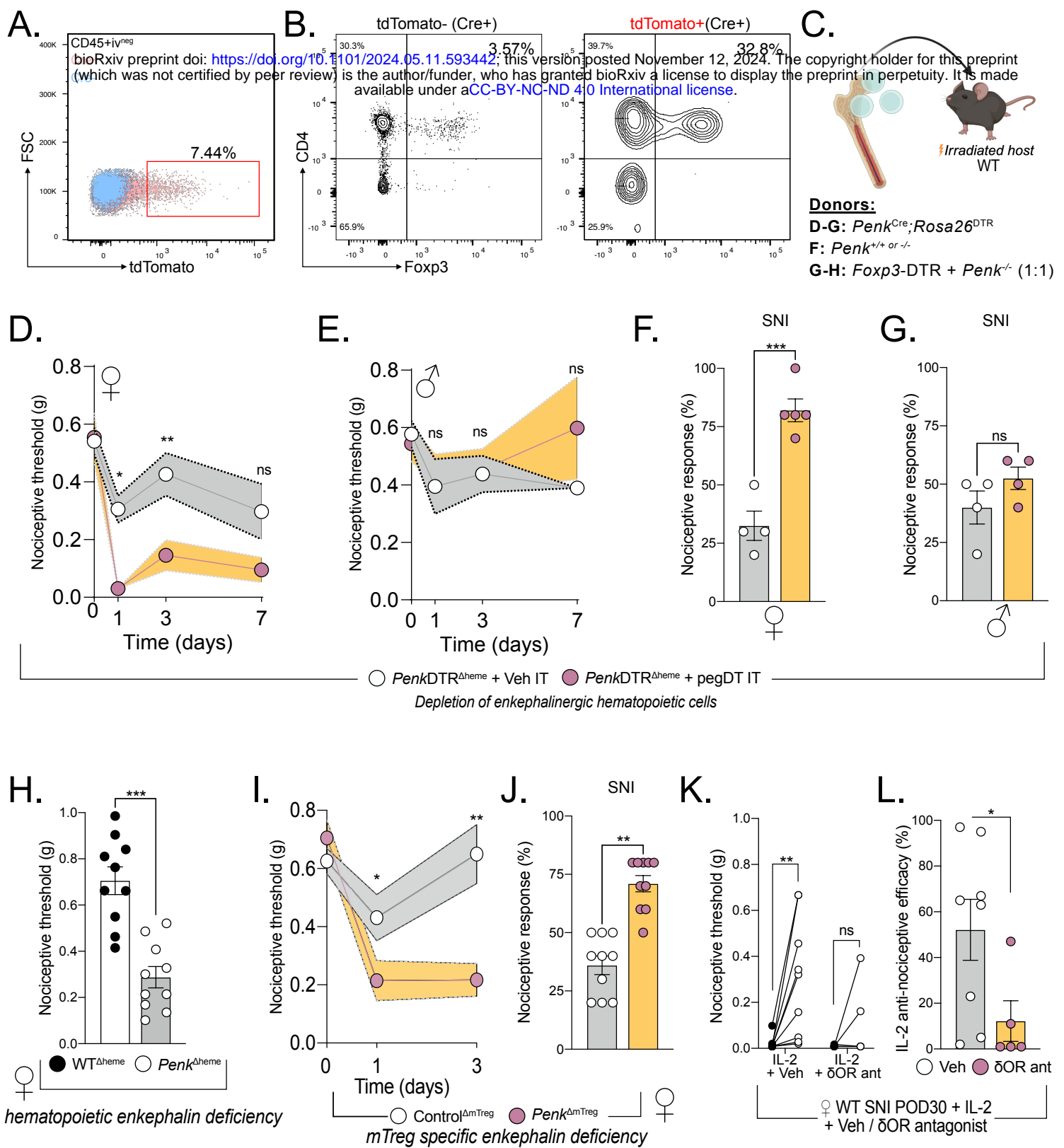
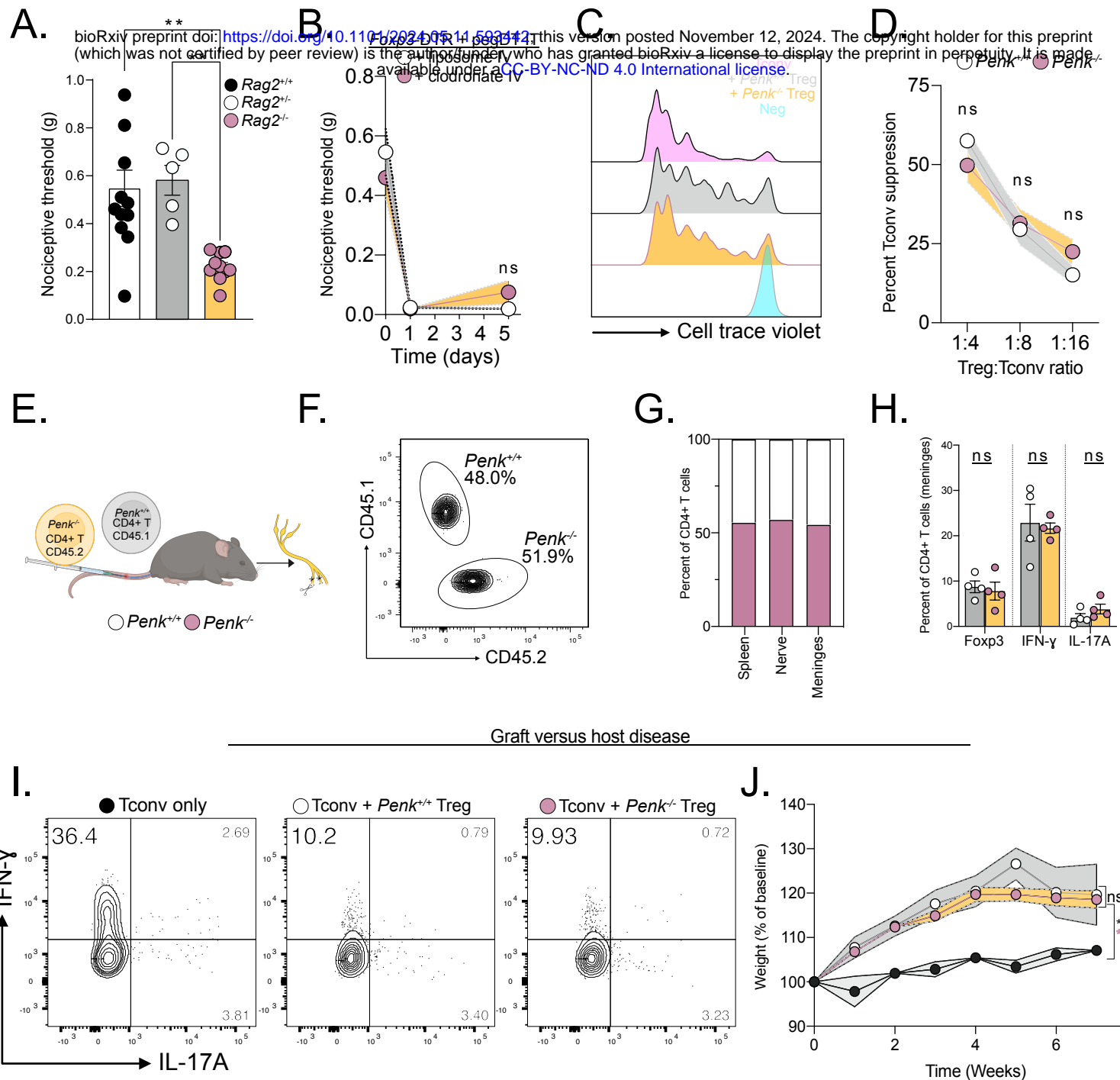
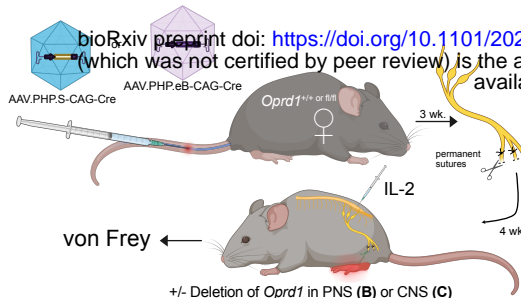


Figure 5

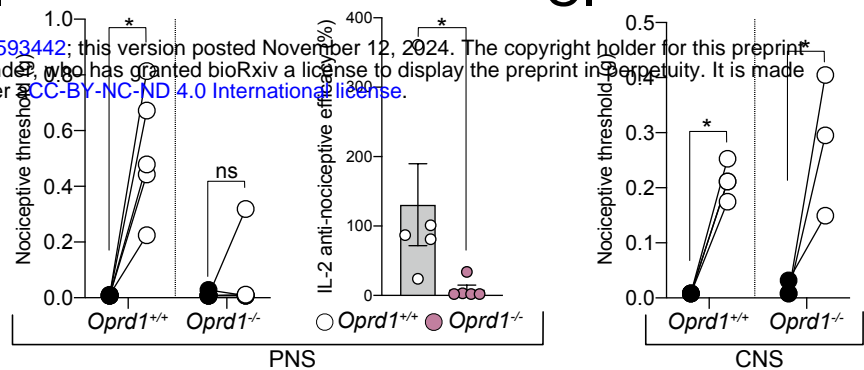
Midavaine et al., 2024



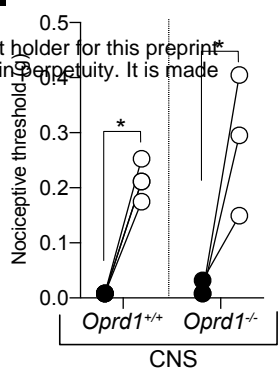
A.



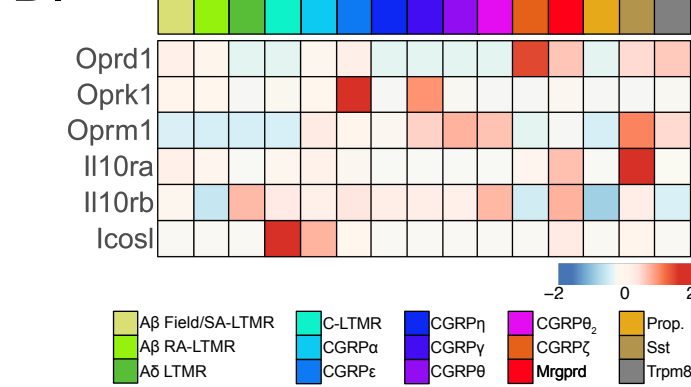
B.



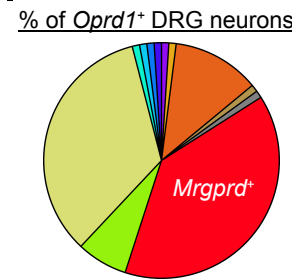
C.



D.



E.



F.

